Nickel aluminate spinel-derived catalysts for the aqueous phase reforming of glycerol: Effect of reduction temperature

A. Morales-Marín[a], J.L. Ayastuy[a,*], U. Iriarte-Velasco[b], M.A. Gutiérrez-Ortiz[a], Chemical Technologies for the Environmental Sustainability Group

[a] Department of Chemical Engineering, Faculty of Science and Technology, University of The Basque Country UPV/EHU, Sarriena S/N, 48940 Leioa, Spain
[b] Department of Chemical Engineering, Faculty of Pharmacy, University of The Basque Country UPV/EHU, Paseo de la Universidad, 7, 01006 Vitoria, Spain

ARTICLE INFO

ABSTRACT

Bulk nickel aluminate ($NiAl_2O_4$) was synthesised by co-precipitation at a Ni/Al mole ratio of 1:2 (stoichiometric ratio). The prepared sample was reduced at different temperatures, in the 300 to 850 °C range, and obtained assays were analysed by a wide range of analytical techniques (XFR, XRD, H_2-chemisoprtion, H_2-TPR, DRS UV–vis NIR, FTIR, ^{27}Al MAS NMR, NH_3-TPD, CO_2-TPD, TPO) and tested for the APR of glycerol. The spinel precursor allowed the formation of small and stable Ni particles (< 14 nm) upon reduction with good performance in the APR of glycerol (NiAl-850 93% conversion, 57% conversion to gas, at 250 °C/45 bar and WHSV 24.5 h^{-1}). Hydrogen was the main gaseous product and the activation temperature did not substantially alter selectivity to gaseous products; however, selectivity to intermediate oxygenated liquid compounds was substantially modified. Overall, glycerol dehydrogenation route was dominant at high reduction temperature. The good stability of the spinel led to stable H_2 yield in the long-term runs (50 h) and proved potential to be used in the APR of glycerol.
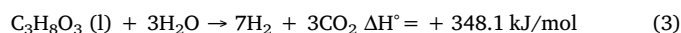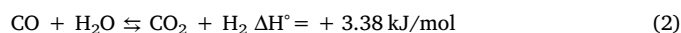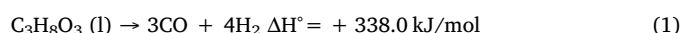
1. Introduction

Glycerol (1,2,3-propanetriol) is a major by-product during the production of biodiesel by transesterification of vegetable oils [1], animal fats [2] and waste oils [3]. Glycerol is generated at approximately 10 wt.% of the total biodiesel produced. Thus, the huge increase in the worldwide production of biodiesel [4] leads to a large amount of glycerol surplus, which must be recycled into higher value-added chemicals for the economic viability of biodiesel industries. The high functionalization of the glycerol molecule makes it prone to many different processes such as oxidation, hydrogenolysis and dehydration [5].

Glycerol can be also used as hydrogen source, as alternative to the traditionally used catalytic steam reforming of methane [6]. The catalytic aqueous phase reforming (APR) of biomass-derived oxygenated hydrocarbons was introduced by first in 2002 by the group of Dumesic [7]. The process can be carried out at relatively low temperatures (200–280 °C) and moderate pressures (15–70 bar) as compared to gas-phase reforming and the selection of proper operation conditions, feedstreams and catalysts can be used to drive the APR to either hydrogen or alkanes production [8]. Thus, undesirable decomposition reactions, such as coke deposition, can be minimized whereas H_2 production can be increased by the Water-Gas Shift reaction (WGS) [6]. APR is also energy-efficient since water and glycerol are not vaporized. Moreover, the concentration of glycerol among the byproducts of biodiesel is optimal to the APR, therefore no pre-treatment is required in order to adjust water/glycerol ratio.

The ideal APR of glycerol yields seven moles of hydrogen and three moles of CO_2 per mole of glycerol (Eqs. 1–3):

$$C_3H_8O_3 \text{ (l)} \rightarrow 3CO + 4H_2 \quad \Delta H° = +338.0 \text{ kJ/mol} \tag{1}$$

$$CO + H_2O \leftrightarrows CO_2 + H_2 \quad \Delta H° = +3.38 \text{ kJ/mol} \tag{2}$$

$$C_3H_8O_3 \text{ (l)} + 3H_2O \rightarrow 7H_2 + 3CO_2 \quad \Delta H° = +348.1 \text{ kJ/mol} \tag{3}$$

A catalyst with high H_2 selectivity must promote C−C and C−H bond cleavage and WGS reaction, and should minimize the C−O cleavage (i.e. CO and CO_2 hydrogenation) [9]. Platinum, ruthenium and in general, metals from Group VIII exhibit high APR activity [10–12]. Benchmark supported platinum catalysts are recognized as the most active and selective catalysts due to their moderate activity in C−C and C−H bond cleavage [6] and low methanation and Fisher-Tropsch activity [8]. In the recent years, nickel based catalysts have attracted considerable attention for the APR process as due to economic criteria

as well as its good intrinsic activity in C—C scission, especially high by small particles [11,13–16]. Nickel supported on conventional γ-alumina has been extensively investigated because of adequate textural properties. However, under APR hydrothermal conditions, γ-Al₂O₃ can be hydrated and transformed into boehmite (γ-AlOOH), with significant alteration of its surface area and acidity. This may provoke activity decay [17] due to dissolution of the support and sinterisation of metal particles [18].

The nature of oxide surfaces that support the metal phase are of critical importance [19,20]. Nickel aluminate (NiAl₂O₄) spinels are known to present a partially inverted structure with part of Ni^{2+} ions occupying octahedral sites and part of Al^{3+} ions tetrahedral ones [21]. On the other hand, the inversion degree of spinels notably affects the nature of the surfaces and also their catalytic properties [22]. The reduction step, indeed, can alter the structural properties. Thus, if metal-support interaction is improved, a better catalytic behaviour could be obtained [23].

In the reduction process of spinel, the oxygen vacancies move through the spinel to the particle surface. As a consequence, changes in the surface microstructure occur, with a major fraction of the nickel metal particles forming on the surface. This way the creation of a nickel aluminate layer between the metallic nickel particles and the alumina could prevent sintering [19]. It has been reported that reduction at high temperatures promotes the rearrangement of nickel in the aluminate matrix, and relatively small Ni crystallites with good textural stability can be obtained [23] what would imply a significant advantage for catalytic applications. It has been reported that reduction of the nickel aluminate leads to metallic Ni in strong interaction with alumina [24].

In this work nickel aluminate spinel was synthesized by coprecipitation at a stoichiometric nickel to alumina mole ratio. It was activated at different reduction temperatures and the catalytic behaviour in glycerol aqueous phase reforming was evaluated. Catalysts characterization was carried out by a wide number of techniques (XRD, UV–visible–NIR DRS, FTIR, ²⁷Al MAS NMR, H₂-TPR, H₂-chemisorption, CO₂-TPD, NH₃-TPD and TPO) and related to the catalytic performance. Adequate nickel speciation and nickel-support interactions were sought in order to attain high selectivity to hydrogen. To the best of our knowledge, the properties and the application of this catalytic system for the glycerol aqueous phase reforming have not been yet investigated.

2. Experimental

2.1. Catalysts preparation

Bulk nickel aluminate (NiAl₂O₄) was synthesised by co-precipitation at a Ni/Al mole ratio of 1:2 (stoichiometric ratio). The procedure was as follows: proper amounts of nickel acetate (99.998% trace metals basis, Sigma-Aldrich) and aluminium nitrate (98.0% purity, Fluka) aqueous solutions were mixed in a vessel at ambient temperature. Aqueous ammonia was added to adjust pH at 8. Solution was continuously stirred for 30 min, while the precipitated was formed. The suspension was kept at ambient temperature for 30 min. The as-prepared solid was filtered, washed thoroughly with distilled water at 90 °C, dried overnight at 110 °C and then calcined at 850 °C (heating rate 10 °C/min, hold 4 h). The as-prepared precursor was divided into six parts. Five were reduced at different temperatures (300, 450, 600, 700 and 850 °C) and remaining part was no further modified. For the characterization where in-situ reduction was not possible, the reduction was carried out ex-situ, in a quartz reactor, under 5%H₂/He flow of 50 mL/min (heating at 10 °C/min, hold 1 h) from room temperature to the desired temperature. Finally, sample was cooled down to room temperature in 5% H₂/He flow. The reduced samples were labeled as NiAl-T, where T indicates the reduction temperature. The unreduced sample was labeled as NiAl-c. Spent catalysts were named as NiAl-T-u (used for 2 h) or NiAl-T-50 h (after 50 h TOS). For comparative purposes, γ-alumina and NiO

were also prepared by simple calcination in air (at 850 °C) of aluminium nitrate and nickel acetate, respectively.

2.2. Characterization techniques

Bulk composition was determined by XRF (AXIOS, PANalytical), by using the fusion method. The amount of leached metals was measured by ICP-AES in the overall liquid sample collected after each reaction. The textural properties were obtained from the nitrogen adsorption-desorption isotherms determined at 77 K in Micromeritics TRISTAR II 3020 equipment. Previously, each sample was outgassed at 300 °C for 10 h, in order to remove moisture and carbon dioxide. The specific surface area and the pore size distribution were determined by the BET and BJH methods, respectively.

The identification of crystalline phases and the morphological study was carried out by X-ray diffraction conducted on a PANalytical Xpert PRO X-ray diffractometer with Cu Kα radiation (λ = 1.5418 Å). Scattered radiation was measured in the range 2θ = 10-80°, with step size 0.026° and a counting time of 2.5 s/step. The crystallite size of each species was estimated from its most intense peak, by using the Scherrer equation. Crystalline phases present in the samples were identified by comparing with the ICDD database.

Exposed metallic Ni atoms per catalyst gram and the Ni metallic surface area were calculated from H₂ chemisorption, carried out in a Micromeritics AutoChem 2920 equipment. Prior to analysis, the samples were heated in He stream at 100 °C, and then reduced under 5% H₂/Ar flow for 2 h at the corresponding reduction temperature. Then the sample was cooled down to 35 °C under Ar flow. Then, H₂ pulses (loop volume 0.5312 mL) were injected until saturation. The exposed metal surface area was calculated assuming H:Ni stoichiometry of 1:1 [25] and spherical Ni particles, with cross-sectional area of 0.065 nm² and density of 8.9 cm³/g [26].

The reducibility of the prepared samples was studied by temperature-programmed reduction (H₂-TPR) in a Micromeritics AutoChem 2920 instrument. For NiAl-c, about 70 mg of sample was initially flushed in 5% O₂-He stream at 550 °C for 1 h (heated at 10 °C/min). It was cooled down to room temperature in Ar flow. Then, a flow of 5% H₂-Ar was passed through the bed containing the sample while temperature was increased to 950 °C at 10 °C/min, and hold for 1 h. The H₂ consumption rate was monitored in a previously calibrated thermal conductivity detector (TCD). The total H₂ consumption measured for sample NiAl-c was defined as TPR-a.

Also, H₂-TPR was carried out for the partially reduced samples (NiAl-T) in order to calculate the fraction of reduced nickel ($f_{Ni,red}$). Firstly, approximately 70 mg of each sample was reduced at temperature T, following the same protocol as for TPR-a. The amount of H₂ consumed in this stage was defined as TPR-b. Then, it was cooled down to room temperature in He flow, and subsequent TPR run, up to 950 °C, was carried out. The amount of H₂ consumed in this stage was defined as TPR-c. The value $f_{Ni,red}$ for each NiAl-T sample was defined as the fraction of the amount of H₂ consumed during its reduction at temperature T (TPR-b) with respect to the total amount of H₂ consumed during the reduction of NiAl-c (TPR-a).

The speciation of nickel cations (coordination and oxidation states) was analysed by Diffuse Reflectance UV–vis spectroscopy with a UV–vis-NIR Cary 5000 equipment coupled to Diffuse Reflectance Internal 2500 within the range 200–2500 nm. Kubelka–Munk function was applied to convert the DRS into equivalent absorption.

Fourier transform infrared spectroscopy (FTIR) transmittance spectra were recorded in the 400-4000 cm⁻¹ range in a Cary 600 Series FTIR apparatus by employing KBr pellet technique, as an average of 50 scans with a resolution of 4 cm⁻¹.

²⁷Al Solid State NMR measurements were performed on a 9.4 T Bruker AVANCE III 400 spectrometer operating at resonance frequencies of 104.26 MHz for 27Al. Chemical shifts were referenced externally to the AlCl₃ aqueous solution at 0 ppm. The spectra were

acquired at a spinning frequency of 60 kHz employing a pH MASDVT400 W BL 1.3 mm ultrafast probehead. A single pulse of 0.3 μs duration was applied and a recycle delay of 0.2 s and 36,000 scans were used.

Surface acidity and basicity were measured by NH_3 pulse chemisorption and CO_2 temperature programmed desorption, respectively. Measurements were carried out in a Micromeritics AutoChem 2920 instrument coupled to Mass Spectroscopy (MKS, Cirrus 3000). About 35 mg of the calcined precursor was initially pretreated in 5%O_2-He stream at 550 °C for 1 h (heating rate 10 °C/ min) and cooled to room temperature. Then, it was reduced at the desired temperature in 5%H_2/Ar flow (heating rate 10 °C/min), hold for 1 h and cooled down in He flow (to 90 °C for NH_3 adsorption and to 40 °C for CO_2 adsorption). For acidity measurements, a series of 10% NH_3-He pulses (loop volume 0.5312 mL) were introduced at 90 °C until constant peak area was achieved. Then, temperature was raised (10 °C/min) to 850 °C into He flow, and the released gases were monitorised by MS (MKS Cirrus) [27]. For basicity measurements, 5% CO_2/He flow was passed through the sample at 40 °C up to saturation. Subsequently, the sample was exposed to a He flow for 60 min at 40 °C in order to remove reversibly and physically bound CO_2. Finally, the temperature was raised to 900 °C (heating rate 10 °C/min) and the resultant signal was followed by MS.

Carbon deposition on spent catalysts was evaluated by temperature-programmed oxidation (Setaram Setsys evolution) coupled to mass spectroscopy (Pffeifer OmniStar) to follow the evolution of m/z signals 44 (CO_2) and 18 (H_2O). Approximately 5 mg of calcium carbonate (used as reference) was added to about 25 mg of sample. The mixture was treated under 5%O_2/He at 150 °C for 1 h and then heated up to 1000 °C at a heating rate of 5 °C/min.

2.3. Catalytic performance evaluation

The aqueous phase reforming (APR) of glycerol was studied in a bench-scale fixed-bed up-flow reactor (Microactivity Effi, PID Eng& TEch). The reactor (i.d. 5.1 mm, height 305 mm) was made of Hastelloy alloy. In a typical run, about 0.5 g of catalyst (particle size 0.04-0.16 mm) were placed on a stainless steel frit and covered with a quartz wool plug. Prior to reaction, it was reduced "in situ", at atmospheric pressure, under 20% H_2 flow (balance He) to the desired reduction temperature, T (heating rate 5 °C/min), and hold for 1 h. Then, He flow was switched to bypass and 10 wt.% glycerol (Panreac, > 99.5% purity) aqueous solution was pumped into the reactor at 0.2 mL/min. Resultant WHSV (determined as the ratio between feed mass-flowrate and mass of fresh catalyst) was of 24.5 h^{-1}. Catalytic performance was measured after two hours of operation. Three temperature/pressure APR conditions were tested: 235 °C/35 bar, 250 °C/45 bar and 260 °C/52 bar. Reaction products were cooled down to 5 °C. The gas products were swept with 40 mL/min of He flow introduced immediately before backpressure regulator, and continuously analyzed by a GC–MS (μGC Agilent, equipped with four columns (Al_2O_3-KCl 10 m, PPQ 10 m, MS5A 10 m, He as carrier and MS5A 10 m, Ar as carrier). The liquid products were analyzed off-line by GC–MS (Agilent, CP-Wax 57CB column) and HPLC-RI (Waters, Hi-Plex H column). Total organic carbon (TOC) in the condensable phase was measured on a Shimadzu TOC-5050 A apparatus.

The total glycerol conversion (X_{Gly}) was calculated as follows:

$$X_{Gly}(\%) = 100 \times \frac{F_{Glycerol}^{in} - F_{Glycerol}^{out}}{F_{Glycerol}^{in}} \tag{4}$$

The carbon conversion to gas (X_{gas}) was calculated as follows:

$$X_{gas}(\%) = 100 \times \frac{F_{C_{atoms,feed}}^{in} - F_{C_{atoms,liquid}}^{out}}{F_{C_{atoms}}^{in}} \tag{5}$$

Selectivity to gas (S_{gas}) was defined as the fraction of carbon moles converted into gas phase per converted glycerol moles:

$$S_{gas}(\%) = 100 \times \frac{F_{C_{atoms,feed}}^{in} - F_{C_{atoms,liquid}}^{out}}{F_{Glycerol}^{in} - F_{Glycerol}^{out}} \times \frac{1}{3} \tag{6}$$

Hydrogen selectivity (S_{H_2}) was defined as the ratio between the moles of hydrogen produced and moles of glycerol reacted, multiplied by 1/7 (inverse of the reforming glycerol/hydrogen ratio, according to reaction (3):

$$S_{H_2}(\%) = 100 \times \frac{F_{H_2}^{out}}{F_{Glycerol}^{in} - F_{Glycerol}^{out}} \times \frac{1}{7} \tag{7}$$

The selectivity of the C-containing product i was calculated as follows:

$$S_i(\%) = 100 \times \frac{F_i^{out}}{F_{Glycerol}^{in} - F_{Glycerol}^{out}} \times \frac{C_{atoms, i}}{3} \tag{8}$$

Finally, hydrogen yield (Y_{H_2}) was defined as the ratio between the moles of hydrogen produced and moles of glycerol fed into the reactor:

$$Y_{H2}(\%) = 100 \times \frac{F_{H2}^{out}}{F_{Glycerol}^{in}} \times \frac{1}{7} \tag{9}$$

3. Results and discussion

3.1. Materials characterization

3.1.1. Chemical composition and textural properties

The experimentally measured nickel loading was 31.3 wt.%, very close to the stoichiometric value (33.2%). Textural properties, detailed in Table 1, revealed that specific surface area of nickel aluminate NiAl-c was very similar to that of bare alumina (101.6 m^2/g, Supporting Information), characteristic of mesoporous solids, with H_2 hysteresis loop, related to disordered porous materials were observed for the prepared assays, irrespective of the reduction temperature. A slight increase in the pore volume, and average pore size (Table S1, Supporting Information), occurred with increasing the reduction temperature. Concomitantly, surface area slightly decreased (S_{BET} 98.0 m^2/g for NiAl-c; 76.6 m^2/g for NiAl-850), likely due to the phase transformation from $NiAl_2O_4$ to Ni/Al_2O_3 [28,29] and the dilution effect. Also, partial blockage of pores cannot be discarded. Overall, this behaviour pointed to a high structural stability of the stoichiometric $NiAl_2O_4$. Pore size distribution (PSD) showed a unimodal structure for all samples (Figure S1B, Supporting Information). It was observed that reduction at above 450 °C shifted PSD to larger values, likely caused by the collapse of the smallest pores.

3.1.2. H_2-TPR and H_2-chemisorption

The reducibility of the nickel aluminate spinel precursor (NiAl-c) and the partially reduced catalysts (NiAl-T) was studied by temperature programmed reduction (H_2-TPR), and the obtained TPR profiles are shown in Fig. 1A. The reduction profile of NiO is also included for comparison. Note that TPR profiles of NiAl-T samples corresponded to the so-called TPR-c, that is, the hydrogen consumption profile of samples previously reduced at temperature T.

NiO exhibited a relatively narrow reduction peak in the 240 °C to 415 °C range, with its maximum at 377 °C. All Ni was reduced at below 400 °C as deduced from the experimentally measured hydrogen consumption of 13.4 mmol$_{H2}$/g (theoretical value 13.3 mmol$_{H2}$/g). Bare γ-Al_2O_3 showed no H_2 consumption in the studied temperature range (not shown). It was clear that incorporation of aluminium significantly modified the reduction profile of NiO. The observed shift in the reduction profile of NiAl-c and that of the partially reduced catalysts evidenced the intimate interaction of Ni with alumina. The left tail suggested the existence of a number of nickel species with different reducibility. The H_2-TPR curve was split into peaks named α, β and γ, for the low, medium and high temperature hydrogen consumption,

Table 1
Textural and structural characteristics of the fresh and spent catalysts.

Sample	Fresh samples							Spent samples						
	S_{BET} (m²/g)	$d_{NiAl2O4}$ [a] (nm)	d_{Ni}^{0} [a] (nm)	Phases detected [a]	Acidity [b] $\mu mol_{NH3}/m^2$	Basicity [c] $\mu mol_{CO2}/m^2$	Acid/ basic sites ratio	S_{BET} (m²/g)	d_{Ni}^{0} [a] (nm)	$d_{boehmite}$ [a] (nm)	Phases detected [a]	Leached Ni [d] (%)	Leached Al [d] (%)	C [e] (mmol_C/g)
NiAl-c	98.0	8.9	n.d.	$NiAl_2O_4$	1.57	0.66	2.4	n.a.	n.a.	n.a.	n.a.	n.a.	n.a.	n.a.
NiAl-300	94.9	9.9	n.d.	$NiAl_2O_4$	1.57	0.59	2.7	102.6	33.9	n.d.	Ni° + $NiAl_2O_4$	0.65	< 0.025	n.a.
NiAl-450	93.5	9.2	n.d.	$NiAl_2O_4$	1.93	0.39	4.9	87.0	30.0	n.d.	Ni° + $NiAl_2O_4$	0.78	< 0.025	n.a.
NiAl-600	89.8	9.8	7.7	Ni° + $NiAl_2O_4$	1.82	0.73	2.3	110.2	45.9	8.1	Ni° + $NiAl_2O_4$ + boehmite	0.72	< 0.025	n.a.
NiAl-700	83.1	9.1	13.6	Ni° + $NiAl_2O_4$	1.70	1.13	1.6	97.4 (92.6)	44.5 (32.0)	15.0 (7.7)	Ni° + $NiAl_2O_4$ + boehmite	0.27 (6.5)	< 0.025 (< 0.025)	(1.12)
NiAl-850	76.6	7.0*	11.6	Ni° + γ-alumina	2.13	1.03	2.0	109.9 (102.9)	41.5 (44.1)	17.4 (7.5)	Ni° + $NiAl_2O_4$ + boehmite	0.19 (5.4)	< 0.025 (< 0.025)	(0.16)

In parentheses, data for experiments with TOS 50 h.
[a] from XRD. [b] from NH₃-TPD. [c] from CO₂-TPD. [d] from ICP-AES. [e] carbonaceous deposits by TPO-MS.
* γ-alumina.

respectively [30]. The α peak was ascribed to the reduction of easily reducible surface free nickel oxide [30], formed in close interaction with the non-stoichiometric nickel aluminate spinels [31]. The medium temperature β peak was ascribed to Ni^{2+} species in a deffective $Ni_{1-x}Al_2O_{4-x}$ phase [32]. Finally, the high temperature peak (γ), centered at 837 °C, was related to the reduction of Ni^{2+} species in the $NiAl_2O_4$ spinel lattice [24]. Free nickel oxide (α peak) was reduced around 150 °C above that of bare NiO, what reflected the strong interaction between NiO particles and the less reducible alumina [33].

Peak β was split into two contributions, namely β_1 (at lower temperature) and β_2 (at higher temperature). The molar ratio β_1/β_2 for the non-reduced sample was 1.10, which, in turn, decreased with the

reduction temperature (Table 2). This suggested that composition of defective $Ni_{1-x}Al_2O_{4-x}$ depends upon reduction treatment, likely β_1 referred to Ni-rich solid and β_2 referred to Ni-lean solid [34].

Hydrogen consumption of β and γ species scarcely varied upon reduction below 450 °C, causing a relative contribution to overall Ni species of around 45% and 52%, respectively. Reduction at 600 °C decreased the hydrogen consumption of the defective spinel phase (β peak) to half, and for NiAl-700 sample Ni^{2+} species in the resultant catalyst were mainly as $NiAl_2O_4$. Eventually, at 850 °C, all Ni added was fully reduced (Table 2, Fig. 1A).

It has been suggested that reduction of α-type NiO produced large Ni particles [32,35]. The quantitative results of the TPR profiles
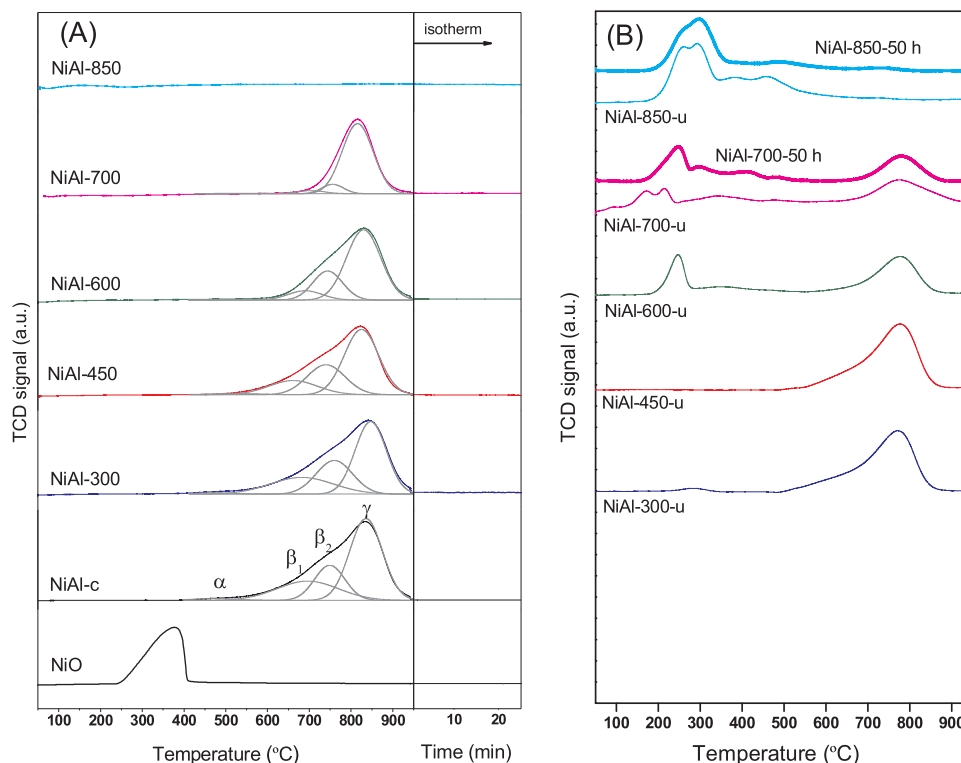

Fig. 1. H₂-TPR profiles for (A) fresh samples; (B) catalysts used in APR reaction: NiAl-T-u: used for 2 h at 235 °C/35 bar; NiAl-T-50 h: used for 50 h at 235 °C/35 bar.

Table 2
Results from H_2-TPR and H_2 chemisorption of the calcined NiAl-c and fresh reduced NiAl-T and used catalysts (2 h TOS).

Sample	Fresh samples										Used samples	
	H_2 consumption (mmolH_2/g)		$f_{Ni,red}$ (%)	Distribution of Ni (mmol Ni/g)						H_2 chemisorption	H_2-TPR	H_2 chemisorption
	TPR-a	TPR-c		As Ni°	As Surface NiO (peak α)	As $Ni_{1-X}Al_2O_{4-X}$ (peak β)	As $NiAl_2O_4$ (peak γ)	mole ratio β_1/β_2		Ni° area (m^2/g_{cat})	Oxidised Ni (%)	Ni° area (m^2/g_{cat})
NiAl-c	5.2	–	–	0 (0.0)	0.08 (1.5)	2.32 (44.7)	2.79 (53.8)	1.10		0	n.a.	n.a.
NiAl-300	–	5.0	3.8	0.20 (3.8)	0.10 (1.9)	2.32 (44.5)	2.59 (49.7)	0.90		0.07	< Q.L.	0.01
NiAl-450	–	4.9	5.8	0.30 (5.9)	n.d	2.19 (42.8)	2.63 (51.4)	0.72		0.10	< Q.L.	0.03
NiAl-600	–	4.1	21.1	1.10 (21.4)	n.d	1.30 (25.3)	2.74 (53.3)	0.47		0.48	124	0.06
NiAl-700	–	2.3	55.8	2.90 (56.2)	n.d	0.30 (5.8)	1.96 (38.0)	0.44		1.63	43 / 34*	0.08
NiAl-850	–	0.01	99.8	5.19 (99.8)	n.d	0 (0)	0.01 (0.2)	0		3.47	45 / 34*	0.23

In parentheses, as mole %.
*, values for 50 h TOS.
Q.L. Quantification level.

(Table 2) showed that α-type species were less than 2% for the catalyst precursor studied here. Thus, the small average crystallite size of Ni° particles obtained (Table 1) could be partially attributed to the lack of" free" nickel oxide species and the fact that catalyst precursor contained mainly Ni^{2+} species in spinel-like structure which favored dispersion of the metallic nickel phase formed upon reduction.

Results from hydrogen pulse chemisorption are given in Table 2. As expected, the accessible metallic nickel surface increased with the reduction temperature from 0.07 m^2_{Ni}/g for NiAl-300 to 3.47 m^2_{Ni}/g for NiAl-850 (in terms of exposed Ni atoms it increased from $1.14 \cdot 10^{18}$ for NiAl-300 to $53.4 \cdot 10^{18}$ at$_{Ni}$/g for NiAl-850), as due to the migration of nickel from spinel phase to the catalyst surface. As shown by TPR, diffusion of Ni^{2+} commenced at around 600 °C (also discussed in XRD and ^{27}Al NMR sections).

3.1.3. XRD characterization

The most prominent features of XRD patterns are ascribed to cubic spinel structure (JCPDS 78–1601) (Fig. 2A). Diffraction line at 2θ = 65.6° (plane (440)) confirmed the formation of $NiAl_2O_4$ spinel. NiO was not detected, probably, because of the smaller than detection limit (2–5 nm) size of the crystallites. Characteristic features of metallic nickel appeared upon reduction at 600 °C or above (2θ = 44.5°, 51.8° and 76.4°) (JCPDS 01-087-0712), and increased in intensity with reduction temperature. It was observed that reduction at ≤ 600 °C hardly altered the XRD spectra peak shape and position (i.e. 2θ = 19.0, 37.0 and 59.6° remained almost constant) reflecting the high stability of the $NiAl_2O_4$ phase. Although TPR analysis confirmed that about 6% of the nickel in the spinel precursor was reduced at 450 °C, its absence in the XRD spectra highlighted an adequate dispersion of the metal. The formation of γ-alumina phase (JCPDS 79-1558) could be recognized upon reduction at 850 °C.

From a structural perspective, the experimentally measured lattice parameter for the unreduced sample was 8.044 Å (Table S2, Supporting Information), very close to that of stoichiometric nickel aluminate spinel (8.0451 Å) [21]. Values of lattice parameter decreased with reduction temperature. This lattice compression reflected the migration of the nickel ions from the nickel aluminate lattice to the surface, suggesting that the solid bulk was progressively enriched in alumina. Upon reduction, metallic nickel crystallized into *Fm-3 m* cubic system (JCPDS 01-087-0712). No evidence was found for hexagonal close packed nickel. At the highest reduction temperature of 850 °C, 2θ position for plane (440) shifted to 67.3° (given as Δθ in Figure S2, Supporting Information), reinforcing the idea that nickel was drawn towards Ni clusters and matrix composition tended to γ-Al_2O_3 [29].

The intensity ratio of peaks corresponding to (220) and (440) reticular planes (I_{220} / I_{440}) (Table S2, Supporting Information) varied among the prepared catalysts. The intensity ratio I_{220} / I_{440} was related to cation distribution [36]. As the ionic radius of Ni^{2+} cation (0.69 Å) exceeds that of Al^{3+} (0.54 Å), I_{220} / I_{440} increases with increasing Ni^{2+} cations on tetrahedral sites (T_d), and the ratio decreases with increasing occupancy of Ni^{2+} cations on octahedral sites (Oh). For "normal" spinel this ratio would approximate to 0.33. We measured a value of 0.25 for NiAl-c (Table S2, Supporting Information), and a decreasing trend with reduction temperature (i.e. I_{220} / I_{440} = 0.21 for sample NiAl-700) was observed. That is, the reduced system was slightly enriched in Ni^{2+} cations hosted in octahedral sites. Therefore, we might conclude that tetrahedral Ni^{2+} cations were more readily reduced as compared to octahedral Ni^{2+} sites. Presumably, the lattice oxide ions of the trigonal prism stabilize the Ni^{2+} ion rather effectively.

Crystallite size of nickel aluminate and metallic nickel (in reduced catalysts) varied in the 9–10 nm and 8–14 nm range, respectively (Table 1). In both cases, no clear trend in crystal growth was observed with the reduction temperature. The relatively small size of the metallic nickel nanoclusters formed in our system, in spite of the high reduction temperature, reflected the strong interaction of nickel with the Ni-Al-O support, which stabilized Ni particles and reduced their surface mobility, protecting against the sinterisation under reductive atmosphere [32,34]. For instance, Ni/alumina catalysts prepared by wet impregnation, and at a similar nickel content, showed a metallic nickel crystallite size of about 26 nm [37].

3.1.4. Skeletal DRS UV–vis NIR and IR characterization

Fig. 3 shows the diffuse reflectance UV–vis NIR spectra of the prepared samples. Main features of NiO spectra include the broad bands in the 900–1400 nm and 250–350 nm regions, ascribed to $O^{2-} \rightarrow Ni^{2+}$ charge transfers [38] and $^3A_{2g} \rightarrow {}^3T_{1g}$ (F) transition bands at 377, 414 and at 720 nm. All these features are characteristic of octahedral Ni^{2+} in NiO lattice [39]. For catalyst NiAl-c, the intensity in the $O^{2-} \rightarrow Ni^{2+}$ charge transfers region increased whereas it was attenuated in the visible range, at around 720 nm, what suggested that Ni^{2+} cations existed in a different electronic environment as compared to bare NiO. The intense doublet, with maxima at 605 and 638 nm, observed for catalyst NiAl-c, was attributed to the $^3T_1 \rightarrow {}^3T_2$ (^3P) spin-allowed transition of Ni^{2+} ions in tetrahedral symmetry (Ni^{2+}_{Td}). Moreover, absorption bands centered at 550 and 760 nm characteristic of Ni^{2+}_{Td} were clearly observed. Thus, these results reflected that Ni^{2+} ions were embedded in the alumina lattice to form $NiAl_2O_4$ phase in the non-reduced NiAl-c sample, in accordance with XRD data.

The DRS UV–vis NIR spectra of partially reduced samples (i.e. ≤ 450 °C) were qualitatively similar to NiAl-c. Reduction at 600 °C removed typical features of NiO and nickel aluminate and only some complex bands at around 330 nm were observed, ascribed to metallic
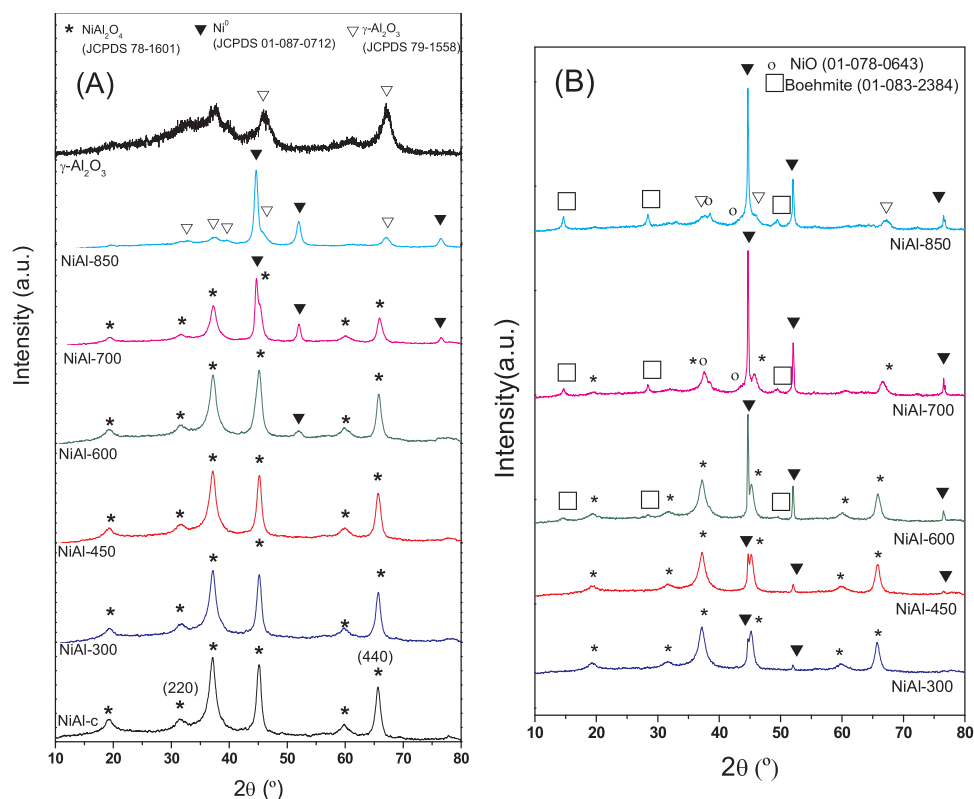
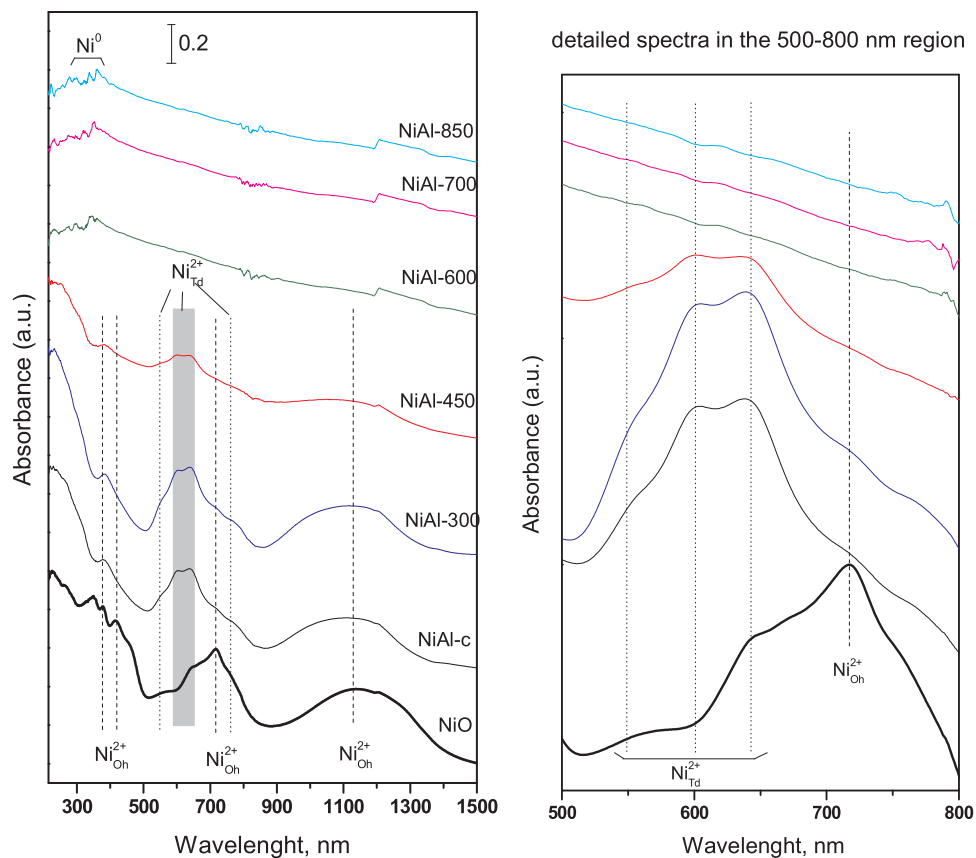**Fig. 2.** XRD spectra of the fresh samples (A) and spent catalysts (B).

Fig. 3. DRS UV–vis NIR spectra of the samples, obtained at ambient temperature, and detailed spectra in the 500–800 nm region.
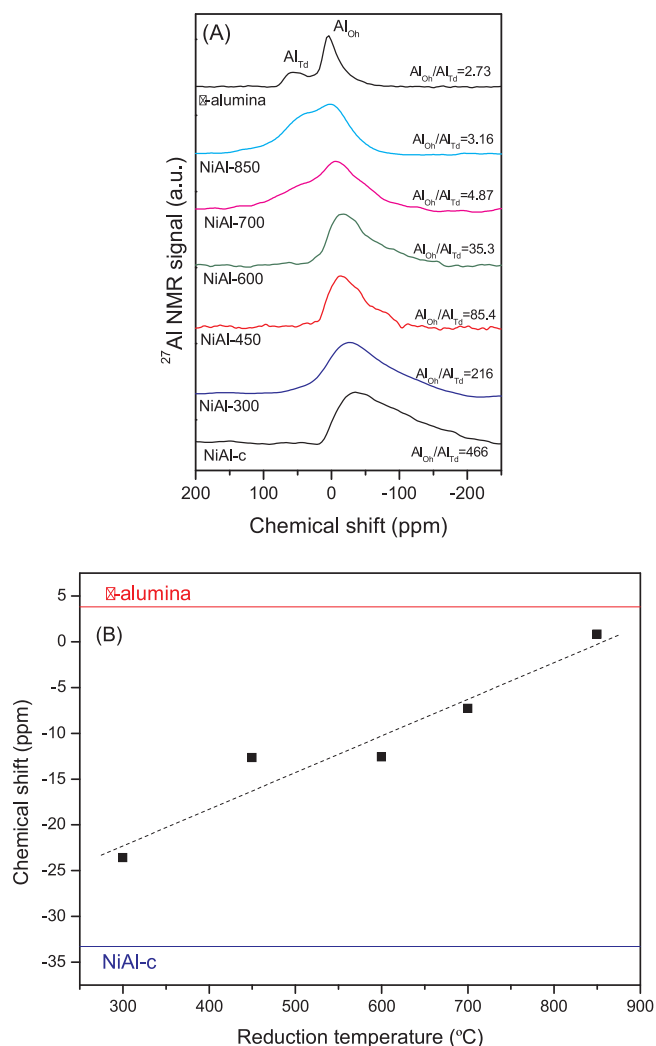
Fig. 4. Chemical shift (A) and variation of chemical shift of Al_{Oh} with reduction temperature (B).

Fig. 5. Surface acid sites density (A) and Surface basic sites density (B).

nickel nanoparticles [40].

The intensity ratio of the doublet at 600–650 nm to peak at 1100 nm ($Ni^{2+}_{Td}/Ni^{2+}_{Oh}$) was used to measure the relative content of Ni^{2+}_{Td} with respect to Ni^{2+}_{Oh} [41]. The experimentally measured values (Table S2, Supporting Information) reflected that the highest $Ni^{2+}_{Td}/Ni^{2+}_{Oh}$ corresponded to sample NiAl-c, and decreased upon reduction, what supports the XRD data.

Further structural characterization carried out by FTIR analysis (Figure S3, Supporting Information) confirmed the above observations. Spinel structure was identified in sample calcined at 850 °C which was readily transformed into γ-alumina under H_2 flow. In the FTIR spectra, alumina could be detected upon reduction above 600 °C (Figure S3A, Supporting Information)

3.1.5. ^{27}Al MAS NMR

Fig. 4A shows the ^{27}Al MAS NMR spectra of NiAl-T samples. The spectrum of γ-Al_2O_3 consisted of two peaks at 3.7 and 60 ppm (i.e. octahedral and tetrahedral aluminium, respectively), with an intensity ratio of 73:27, as also reported by others [42].

The non-reduced assay showed a broad peak centered at -33 ppm, reflecting the predominant existence of Al_{Oh}. The subtle peak at around 70 ppm denoted the presence of Al_{Td}, characteristic of partially inverted spinels. Reduction at below 600 °C hardly varied the Al-NMR spectra, and Al^{3+} mainly occupied the octahedral sites. However, reduction at above 600 °C increased the amount of Al_{Td} in the catalyst, as deduced
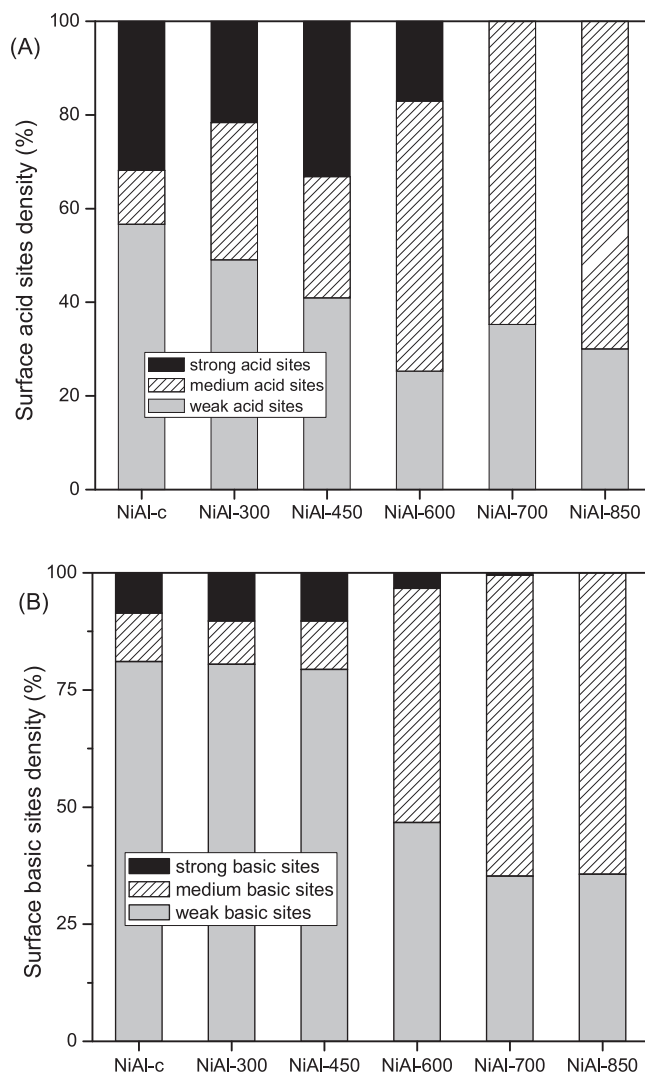
from the enlarged signal at around 60 ppm. This is consistent with the departure of Ni^{2+} to octahedral sites to ensure neutrality. Indeed, Fig. 4B shows that Al_{Oh} chemical shift linearly increased with the reduction temperature, which was bottom and upper limited by NiAl-c (-33.3 ppm) and γ-alumina (+ 3.8 ppm). For NiAl-850 sample, δ_{AlOh} was + 0.8 ppm, close to γ-alumina.

3.1.6. Surface acidity and basicity

Aqueous phase reforming of glycerol involves, among others, dehydration reactions [15], which are very sensitive to catalysts surface acid-base properties [43]. Therefore, the study of the total amount and strength of such functionalities could help the interpretation of the activity and selectivity data. Results from CO_2 and NH_3 chemisorption are given in Table 1 and Fig. 5.

Activation under hydrogen flow increased acidity, up to 35% (highest value for NiAl-850: 2.13 $\mu mol_{NH3}/m^2$). The increase of surface basicity was even more marked, up to a two-fold increase, especially at the most severe reduction conditions. The fact that strong sites decreased during reduction suggested that exposed coordinatively unsaturated nickel cations and oxygen species in the calcined spinel may act as strong acid and basic sites, respectively. Treatment under hydrogen flow caused surface enrichment in medium strength sites. This was probably due to the progressive dehydroxylation of the surface and increase of exposed γ-alumina on surface, as revealed by XRD, FTIR and ^{27}Al MAS NMR. Actually, reduction at above 600 °C completely

removed strong sites. Moreover, it has been reported that reduced Ni could react with strong acid sites and generate Ni^{2+} ions (as NiO), which increase the middle-strength acidity [44]. The observed complexity in the medium strength desorption region as reduction temperature increased (Figure S4, Supporting Information) could be ascribed to modification of the oxygen coordination in the catalyst surface. Overall, based on the APR selectivity data discussed later, it can be deemed that these differences in the acid-base properties were sufficient to change catalyst performance.

3.1.7. General overview of the catalysts physico-chemical properties upon reduction

Nickel species of different reducibility were found in the nearly stoichiometric $NiAl_2O_4$ prepared by coprecipitation: (i) a small fraction of surface free nickel oxide, without interaction with the support, which vanishes after reduction above 300 °C; (ii) two kinds of Ni^{2+} species in defective $Ni_{1-X}Al_2O_{4-X}$ (one in Ni-rich and the other in Al-rich environment) which contribution decreased upon reduction at above 600 °C; and (iii) nickel in spinel phase, which can only be completely reduced at 850 °C or above. Based on H_2-TPR data, Ni^{2+} species in Ni-rich mixed oxide phase (peak β_1), were more reducible [29]. Reduced Ni^{2+} species migrated to the solid surface leading to a framework enriched in Ni^{2+} species in Al-rich mixed oxide phase (β_2), as suggested by the decrease of the β_1/β_2 ratio (Table 2).

Under H_2 atmosphere, nickel diffused through the lattice of the non-stoichiometric spinel to form metallic Ni (Table 2). Ni diffusion continued until $Ni_{1-X}Al_2O_{4-X}$ was completely reduced, at around 700 °C. Above that temperature, further Ni diffusion proceeded from stoichiometric $NiAl_2O_4$. A similar behaviour was observed by Braidy et al. [34] with Ni doped alumina spinels prepared by wet-incipient method. They proposed that under reductive atmosphere, a continuous transition between $Ni_{1-X}Al_2O_{4-X}$ towards γ-alumina occurs as Ni leaves the matrix to form $NiAl_2O_4$ and eventually Ni. The intermediate formation of $NiAl_2O_4$ before metallic Ni, could explain the observed upturn in the contribution of $NiAl_2O_4$ in the NiAl-T series (Table 2). Previous research [24,29], based on H_2-TPR analyses, concluded that Ni located in tetrahedral sites could be more difficult to reduce than Ni located in octahedral sites. Nevertheless, based on XRD, DRS-UV–vis and ^{27}Al-NMR data of our stoichiometric nickel aluminate spinels a different behaviour could be evidenced. That is, upon reduction, the number of tetrahedral nickel atoms diminished and increased that in octahedral sites). Regarding surface acid/basic properties, treatment under hydrogen flow caused surface enrichment in medium strength sites.

3.2. Catalytic performance experiments

Catalytic APR tests were performed at 250 °C/45 bar in a bench-scale fixed-bed up-flow reactor. Bare γ-alumina and NiAl-c showed null activity (not shown). Blank tests with the reactor bed filled with quartz wool (employed to keep the bed fixed) showed no glycerol conversion, which suggested that homogeneous APR had no contribution to the catalytic conversion of glycerol. As a reference, the activity of bare Ni (obtained by reduction of NiO at 700 °C for 1 h) was also evaluated.

Glycerol conversion (X_{Gly}) and carbon conversion to gas (X_{gas}) of NiAl-T catalysts in-situ reduced at temperature T are displayed in Fig. 6A. Aqueous phase reforming of glycerol was negligible by reduced bare Ni catalysts which did not surpass conversion values of 3%. Raney Ni has been reported to be active for APR [45]. The very low performance of our bare nickel catalyst (in terms of X_{Gly} and X_{gas}) could be ascribed to its low surface area (less than 5 m²/g).

Similarly, values for NiAl-350 and NiAl-450 remained below 5%. However, catalytic activity notably increased by increasing the catalysts' reduction temperature from 450 °C to 600 °C. For instance, glycerol conversion increased by a factor of 20 (NiAl-600: X_{Gly} = 66%). The most active assay was that reduced at 850 °C with X_{Gly} = 93% (i.e. X_{Gly} increased by a factor of 1.4 with respect to NiAl-600). In addition,
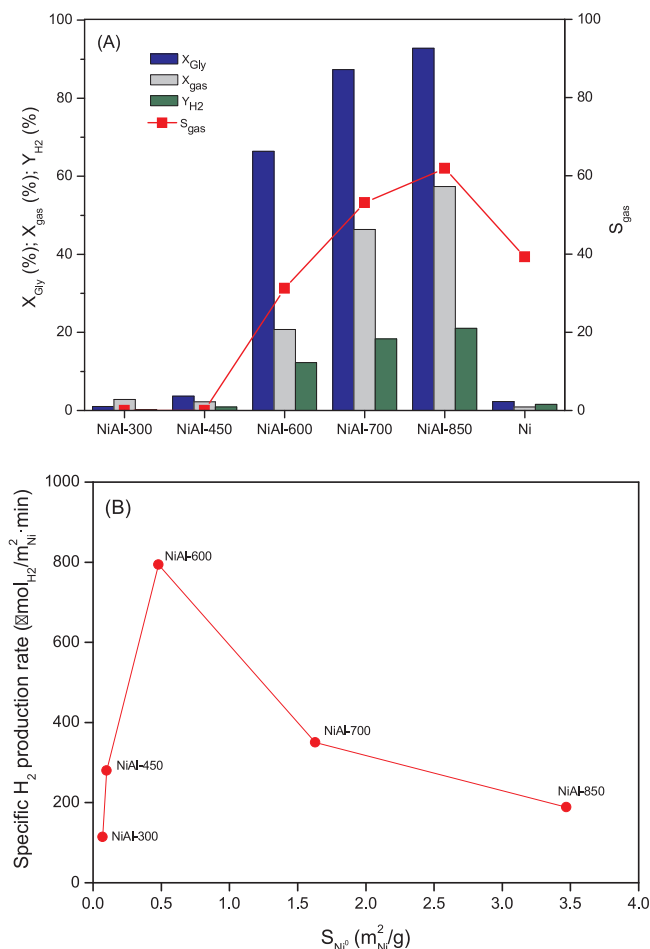

Fig. 6. (A) Glycerol conversion, conversion to gas, hydrogen yield and selectivity to gas. (B) Specific hydrogen production rate. Reaction conditions: 250 °C/45 bar (0.5 g of catalysts, feed rate 0.2 mL/min, 10 wt.% glycerol in water mixture, WHSV = 24.5 h⁻¹, data at steady state = 2 h).

reduction at the highest temperature had a positive effect on the formation of gaseous products. The selectivity to gas (S_{gas}), that is, the percentage of carbon moles converted into gas phase per converted glycerol moles, was doubled in this temperature range: NiAl-600 (31%); NiAl-850 (62%), Fig. 6A. Concomitantly, the exposed Ni metallic area increased by a factor of 5 (Table 2), NiAl-600/NiAl-450 = 0.48/0.10). Thus, the role of the available Ni° in the reforming activity seemed evident. At this point, it is interesting to note that the specific rate of hydrogen production, defined as the rate of hydrogen production per accessible nickel area, was maximum for NiAl-600 (Fig. 6B), which could be ascribed to its smallest metallic particle size (Table 1). It has been reported that partial oxidation of the surface of catalyst and the presence of metal oxide can facilitate dehydrogenation reactions [46]. Regarding particle size, both reforming and WGS reactions involve activation of water molecule. Alumina is able to activate water by forming hydroxyl groups. Nickel, in contrast to other metals such as Pt [47], is also capable of activating water via NiO formation [48]. Therefore, reactive Ni sites should be in close proximity to alumina, what would be more feasible over the smallest Ni particles.

Data on Table 3 provide a comparison of the catalytic performance of our samples and others reported in the literature. In general terms, it is remarkable the high performance shown by our nickel aluminate catalysts when comparing with other nickel-based catalysts, in spite of the high space velocity (WHSV 24.5 h⁻¹) employed. The performance in terms of activity of our catalysts was even comparable to Pt-based catalysts, though, at lower selectivity to hydrogen, due to the inherent

Table 3
Comparison of the performance of nickel aluminate spinel-derives catalysts with other researches for APR of glycerol.

T (ºC)/ P (bar)	Reactor	Catalyst	Feed, WHSV or gly/cat	X_{Gly} (%)	X_{gas} (%)	S_{H2} (%)	Y_{H2} (%)	S_{gas} (%)	Ref.
250/50	Fixed-bed	Ni/Al$_2$O$_3$, CP, 5% Ni	10% gly/w, 2.45 h^{-1}	67	87	–	–	43	[49]
250/50	Fixed-bed	Ni/Al$_2$O$_3$, IMP, 10% Ni	10% gly/w, 2.6 h^{-1}	40	10	–	–	25	[9]
250/20	Fixed-bed	Ni/LaAlO$_3$, DP, 15% Ni	15% gly/w, 5.2 h^{-1}	23	–	61	–	–	[50]
240/40	Fixed-bed	Ni/CeO$_2$/Al$_2$O$_3$, IMP, 6% Ni, 3% CeO$_2$	1% gly/w, 12 h^{-1}	26	–	49	12	–	[51]
250/35	Fixed-bed	Ni/HTLC, CP, 20% Ni, Al/Al + Mg = 0.24	10% gly/w, 5.1 h^{-1}	30	16	31	10	18	[13]
250/25	Fixed-bed	Ni/Ce$_{0.3}$Zr$_{0.7}$O$_2$, CP, 10% Ni	10% gly/w, 2.45 h^{-1}	90	99	–	–	37	[52]
225/28	Microreactor Fixed-bed	Pt-Re/AC, IMP, 3%Pt, 3%Re	10% gly/w, 5.0 h^{-1}	88	58	24.5	–	22	[53]
250/45	Batch	Pt-K/HT, IMP, 1%Pt, 2.8%K	10% gly/w gly/cat = 0.1, t = 4 h	88	87	–	48	33	[54]
225/27.6	Fixed bed	Pt/MgO, IMP, 0.79% Pt	5% gly/w, 3.6 h^{-1}	–	38	60	28	–	[55]
250/45	Fixed bed	NiAl$_2$O$_4$, CP, 33% Ni	10% gly/w, 24.5 h^{-1}	93	57	23	21	62	This work

gly/w: glycerol to water weight ratio in the feed, continuous reactor.
gly/cat: glycerol to catalyst weight ratio in the feed, batch reactor.
t: reaction time, batch reactor.
HTLC: hydrotalcite-like compound.
AC: activated carbon.
IMP: impregnation.
DP: deposition-precipitation.
CP: coprecipitation.

methanation activity of Ni. Indeed, it would be of interest to focus future research on increasing the selectivity to hydrogen (decrease selectivity to alkanes) of nickel aluminate-based catalytic system.

3.2.1. Gas phase products

The main products in the gas phase were hydrogen, carbon dioxide and methane, which accounted for more than 97% of the reaction products (in mol %), for all catalysts. Other minor compounds detected in the gas phase were alkanes (ethane, propane and C$_{4+}$) and carbon monoxide. Molar flow of gaseous products by catalysts NiAl-300 and NiAl-450 was very low, around 30 times lower than most active assays (Fig. 7). The former catalysts produced a gas stream mainly composed by hydrogen (80–90% H$_2$). However, due to their low activity, because active sites are known to be the metallic nickel sites, hydrogen yield was very low (Y_{H2} = 0.7–1.4%, Table 4). For the catalysts reduced at 600 °C or above, hydrogen yield notably increased (up to 21%) what, subsequently, favoured hydrogenolysis and hydrogenation reactions [56], as discussed in the liquid products section. Consequently, hydrogen concentration in the gas stream decreased, and levelled-off, at around 40–50% with a moderate formation of methane (i.e. 22%). It seems interesting to note that activity increased with reduction temperature in the 600 °C–850 °C interval (i.e. amount of active sites increased, Table 2), however, the gas phase composition remained quite

Fig. 7. Gas phase composition (dry basis) (in bars), and total gas flow (line).

similar (Fig. 7), what suggests that reaction mechanism did not vary substantially among the most active assays.

The C—C scission ability of nickel was clearly evidenced from the large difference observed in the selectivity of C$_1$ (methane) and C$_2$ + C$_3$ alkanes (Table 4, Figure S5, Supporting Information), which implies that C—C scission activity was higher than dehydration/hydrogenation of the intermediate liquid compounds [57]. These results also suggested that a minimum amount of metallic Ni was required on catalyst surface to drive hydrogenolysis reactions. The metallic sites would ensure sufficient in-situ produced hydrogen for the hydrogenation of the liquid intermediate hydroxyacetone molecule. For instance, catalyst NiAl-450, with 0.1 m$^2_{Ni}$/g, mainly produced C$_3$ alkanes. This sample presented the highest acid to basic sites ratio (4.9, Table 1) which is beneficial for cleavage of C–O bonds [58]. However, catalyst NiAl-600 ($\sim$0.5 m$^2_{Ni}$/g) showed a selectivity of 17% to C$_1$ alkane (methane), with negligible formation of C$_2$ and C$_3$ alkanes. According to reaction network proposed (Scheme 1), methane was formed by CO hydrogenation, which requires metallic sites. The formation of methane was thermodynamically favoured, as CO hydrogenation reaction to methane is exothermic. As revealed by data in Table 4, H$_2$/CO$_2$ ratio remained below 7/3 (stoichiometric ratio in APR of glycerol) and decreased with reduction temperature. Indeed, this result supports that hydrogen was readily used in parallel reactions. Decarbonylation of intermediate liquid organic compounds formed CO molecules, which undergo WGS reaction to produce CO$_2$ and H$_2$ (Scheme 1). Indeed, Ni-based catalysts are reported to be active for the WGS reaction [59]. The low amount of CO obtained with our samples (Table 4) suggested that WGS was also favoured by NiAl$_2$O$_4$-derived catalysts to form H$_2$ and CO$_2$. C2 and higher alkanes could be formed through Fischer-Tropsch [8] and other reactions. For example, dehydration/hydrogenation of light alcohols can produce ethane and propane, while condensation reactions of intermediate liquid products can yield butane [60].

3.2.2. Liquid phase products

Molar flow of liquid products was negligible for catalysts NiAl-300 and NiAl-450, as well as for bare Ni, as due to their low catalytic activity. Catalyst reduced at 600 °C produced around 0.7 mmol$_C$/g$_{cat}$·min of intermediate liquid products, which slightly decreased by increasing the reduction temperature (i.e. 0.53 mmol$_C$/g$_{cat}$·min for NiAl-850) (Fig. 8A). This decline was ascribed to gasification of intermediate oxygenated hydrocarbon species by reforming reactions [8,61], as deduced from the concomitant increase in the conversion to gas.
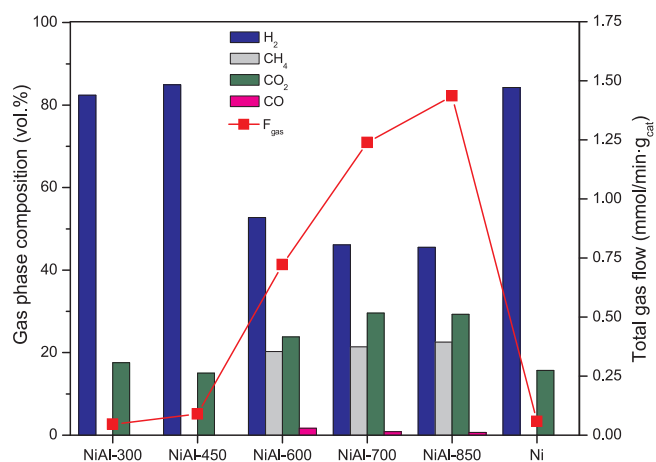
Table 4
Experimental results for the APR of 10 wt% glycerol at 250 °C and 45 bar over NiAl-T catalysts for 2 h.

Catalyst	S_{gas} (%)	S_{H2} (%)	S_{CH4} (%)	H_2/CO_2	CO/H_2	Y_{H2} (%)	S_{C2} (%)	S_{C3} (%)
NiAl-300	∼0	95	0	4.7	0	0.7	0	0
NiAl-450	∼0	90	0	5.6	0	1.4	0	4.95
NiAl-600	31.2	18	17	2.2	0.032	12.3	0.44	0.23
NiAl-700	53.1	21	23	1.6	0.018	18.4	0.47	0.27
NiAl-850	61.9	23	26	1.6	0.015	21.1	0.43	0.23
Ni	39.1	56	0	5.4	0.00	1.58	0	0

The reaction network (Scheme 1) for the glycerol APR over bi-functional NiAl-T catalysts comprises two main routes: dehydrogenation to glyceraldehyde (route A), which requires metal sites, and dehydration to hydroxyacetone (route B), which requires acid sites. It is widely accepted that hydroxyacetone is formed by elimination of primary hydroxyl group of glycerol, while 3hydroxypropanal is formed by elimination of secondary hydroxyl group [62]. The fact that the later was no detected, was ascribed to the preponderant Lewis type acidity of our solids [62].

According to Fig. 8A, the catalyst activation temperature strongly affected the selectivity to the liquid products. Catalysts reduced at low temperature (NiAl-300 and NiAl-450) mainly produced hydroxyacetone and very low amounts of small chain mono-alcohols (ethanol, methanol), suggesting that these catalysts favour dehydration reactions, as due to the scarcity of accessible nickel surface. The acid function was dominant in these catalysts (as revealed by a high ratio of acid/base sites). Consequently, hydroxyacetone was hardly hydrogenated to propylene glycol. In contrast, bare Ni, with only metallic function, produced a liquid stream mainly composed by methanol (73%) and an hydrogen-rich gaseous stream. According to Scheme 1, methanol was formed through decarbonylation reactions (route A), with CO (and H_2) release, which would be subsequently converted by WGS to yield more hydrogen and CO_2.

For catalysts reduced at 600 °C or above, the main liquid products were glycols (1,2-propylene glycol and ethylene glycol), small chain mono-alcohols (ethanol and methanol), hydroxyacetone and, acetaldehyde in much lesser concentration. The observed liquid products distribution pointed to a complex process, where dehydrogenation, dehydration and hydrogenolysis reactions take place [6].

It should be noted that large amounts of glycols (sum of ethylene glycol and 1,2-propylene glycol) were produced, in the 47–59% range

(Fig. 8A), by all the active assays, indicative of C—O (i.e. 1,3-propylene glycol) and C—H and C—C (i.e. ethylene glycol) bond scission over Ni sites. Small amounts of 1-propanol and 2-propanol were also detected (less than 2%). These can be produced by additional dehydration and hydrogenation of 1,2-propylene glycol in the presence of hydrogen [63].

Liquid phase product distribution was notably affected by the catalyst activation temperature. Production of 1,2-propylene glycol and hydroxyacetone decreased as reduction temperature increased (1,2-propylene glycol: from 44% to 29%; hydroxyacetone: from 16% to 7%, both cases by NiAl-600 and NiAl-850, respectively). In contrast, the production of methanol and ethanol increased in similar intensity.

Fig. 8B shows the evolution of the overall reaction products of route A with respect to all reaction products of route B. That is, the sum of total products of dehydrogenation (methanol, ethylene glycol and ethanol) and dehydration (hydroxyacetone and 1,2-propylene glycol) reactions are depicted. A clear trend could be observed where an increase in the reduction temperature enhanced the production of dehydrogenation products. In contrast, a concomitant decrease of dehydration/hydrogenation products could be confirmed. For instance, for catalysts reduced at below 600 °C dehydration/hydrogenation products accounted for 39% of APR products, which increased up to 61% at the highest reduction temperature. From Fig. 8B it could be concluded that at above 700 °C, route A prevailed. This confirms the relevant role of metallic sites in determining the dominant route in the APR of glycerol. The fact that route A (dehydrogenation-decarbonylation) was the main mechanism reflected that C–H and C–C scission by hydrogenolysis was favoured, in detriment of CO cleavage, as also reported by others [64]. Gandarias et al. [65] studied the effect of the incorporation of Cu into Ni/Al_2O_3 catalysts. They concluded that the reduction in size of the Ni ensembles inhibited the C—C bond cleavage. This effect should not be
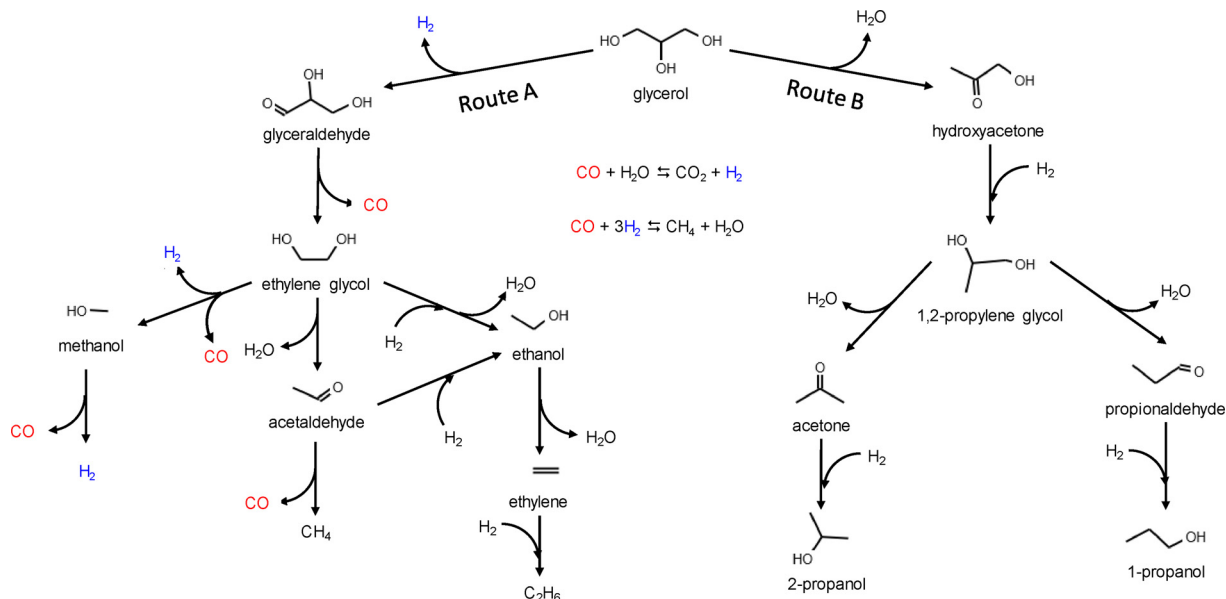
Scheme 1. Reaction pathway proposed for the glycerol APR on nickel aluminate spinel-derived nickel catalysts.
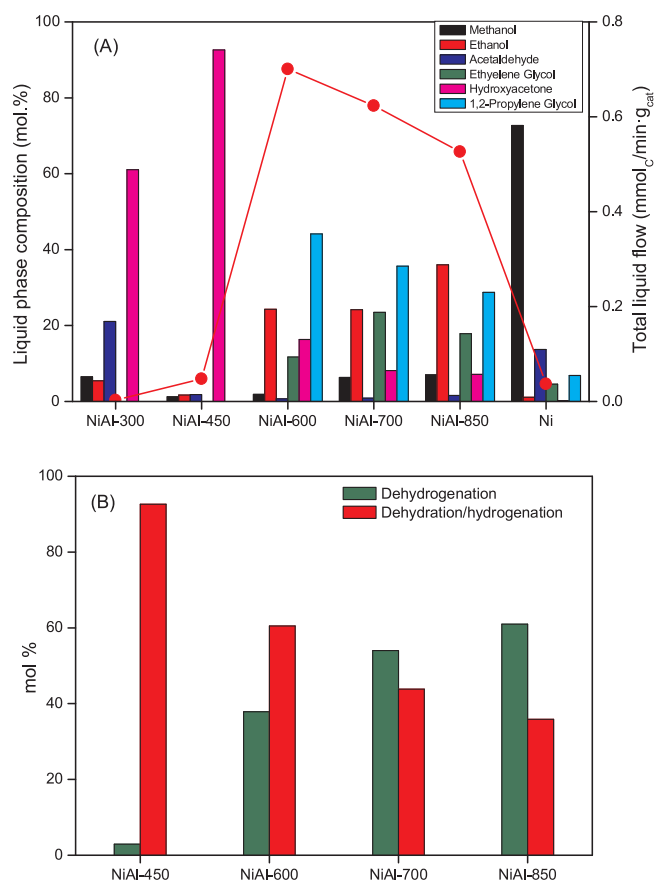
Fig. 8. (A) Molar composition of the main liquid products, and (B) mole distribution between products of dehydrogenation and dehydration/hydrogenation. Reaction conditions: 250 °C/45 bar (0.5 g of catalysts, feed rate 0.2 mL/min, 10 wt.% glycerol in water mixture, WHSV = 24.5 h^{-1}, data at steady state = 2 h).

discarded for our catalytic system.

The formation of Ni−C bond requires a previous dehydrogenation of glycerol in order to be adsorbed on Ni metal [64]. The high selectivity to hydroxyacetone suggested that this mechanism prevailed for catalyst NiAl-300 and NiAl-450, probably due to its low hydrogen yield. If hydrogen partial pressure increases (i.e. due to in-situ formation), both hydrogen and glycerol can adsorb on Ni sites. Then, after protonation of hydroxyl group by metallic acidic sites [66], the cleavage of C−O bond would proceed followed by hydrogen transfer from Ni to the carbon, resulting in 1,2-propylene glycol formation, which was observed for catalysts reduced at 600 °C or above. The occurrence of this route would be supported by the presence of propanols, which were formed through the dehydration/hydrogenation of 1,2-propylene glycol (Scheme 1). However, the small amounts of propanols and acetone (less than 0.8 mol%) reflected the 1,2-propylene glycol was the final liquid product by this route, since further decomposition would require acid sites for dehydration to acetone or propionaldehyde. Experimental data pointed to the preponderance of metallic function with respect to acid function in the investigated catalytic system.

Ethanol can be formed through hydrogenation of the acetaldehyde molecule [67] (Scheme 1). The low amount of acetaldehyde produced by our active catalysts revealed the feasibility of this route. By increasing reduction temperature, H$_2$/CO$_2$ ratio slightly decreased, as shown in Table 4, as the yield to ethanol increased. This result suggested that for catalysts reduced at the highest temperatures (700 and 850 °C) hydrogen yield increased, however, a larger fraction of the in-situ formed hydrogen was consumed in hydrogenolysis reactions. Catalyst NiAl-850 showed to be the best catalyst in terms of glycerol

conversion and hydrogen yield for the aqueous phase reforming of 10 wt.% glycerol. However, it seems interesting to note that the intrinsic activity of the Ni active sites was largest for NiAl-600 (Fig. 6B). It could be concluded that catalyst reduced at the highest temperature consumed more hydrogen in parallel reactions with superior methane formation. It would be of interest to gain knowledge on the properties required to improve the intrinsic activity of the catalyst reduced at the highest temperature. It is likely that adequate surface acid/base properties of the nickel aluminate catalyst could allow tuning the selectivity towards dehydrogenation reactions rather than hydrogenolysis.

3.2.3. Effect of working Temperature/Pressure conditions

Catalytic tests were performed at 235 °C/35 bar, 250 °C/45 bar and 260 °C/52 bar over in-situ reduced NiAl-T catalysts. As shown in Fig. 9A (and Table S3, Supporting Information), independent of the operation conditions, activity was negligible for catalysts NiAl-350 and NiAl-450, which did not surpass conversion values of 5%. The performance of the rest of catalysts, in terms of conversion of glycerol and gasification activity, improved at the most severe APR conditions, in agreement with literature [13,46]. For example, X$_{gas}$ increased by 31% (NiAl-450), 63% (NiAl-600), 74% (NiAl-700) and 79% (NiAl-850) by changing from 235 °C/35 bar to 260 °C/52 bar. Concomitantly, S$_{gas}$ increased by 22% (NiAl-600), 30% (NiAl-700) and 38% (NiAl-850). Hydrogen yield also increased (Table S3, Supporting Information), due to enhanced C−C and C−O bond cleavage promoted by temperature increase [68,69].

Apparent activation energy was estimated assuming first order reaction kinetics. The obtained values (Fig. 9A), ranged between 75–110 kJ/mol, reflecting the weight of catalyst configuration on reaction mechanism. The increasing trend in the Ea suggests that the reactions over metallic nickel sites were characterized by a higher activation energy than those occurring over the acid sites.

The concentration of H$_2$ and CH$_4$ in the gas stream (Table S3, Supporting Information) slightly varied with T/P conditions, and a trade-off could be deduced between both species. This way, as T/P varied from 235 °C/35 bar to 260 °C/52 bar, the H$_2$ concentration in the gas stream vaguely decreased: 54% to 52% (NiAl-600); 53% to 45% (NiAl-700); 48% to 43% (NiAl-850), while CH$_4$ concentration increased as: 20% to 21% (NiAl-600); 19% to 24% (NiAl-700); 20% to 25% (NiAl-850). Accordingly, H$_2$/CO$_2$ ratio declined (Table S3, Supporting Information) what reflected hydrogen consumption in parallel reactions, such as CO methanation, as revealed by increased selectivity to methane.

The alkane selectivity as a function of C number followed similar distribution with reaction T/P, the highest selectivity being for C1 alkanes (methane) for the three T/P operation conditions (Figure S5, Supporting Information). At most severe conditions selectivity to methane increased, especially at the highest reduction temperature.

Liquid phase composition of active catalysts also varied with the reaction T/P conditions (Fig. 9B), while for catalyst NiAl-450 it was almost unaffected. Moreover, the effect of T/P became more intense as reduction temperature increased (i.e. the activation energy). A trade-off between small chain alcohols (which increased) and glycols (which decreased) was observed with the increase of T/P, with almost constant formation of hydroxyacetone.

The ratio between overall reaction products of route A with respect to route B was above 1 for NiAl700 and NiAl850 catalysts, and below 1 for the rest of catalysts. In addition, it increased with reaction T/P conditions, except for NiAl-450 (Figure S6, Supporting Information). For example, changing from 235 °C/35 bar to 260 °C/52 bar, it increased from 1.1 to 2.9 for NiAl-850 catalyst, and at lesser extent for NiAl-600 (from 0.5 to 0.7). This behaviour could be interpreted as that most severe conditions favoured decarbonylation and C−C scission over C−O scission [70].

3.2.4. Long-term experiments

Catalytic performance (i.e. glycerol conversion, conversion to gas
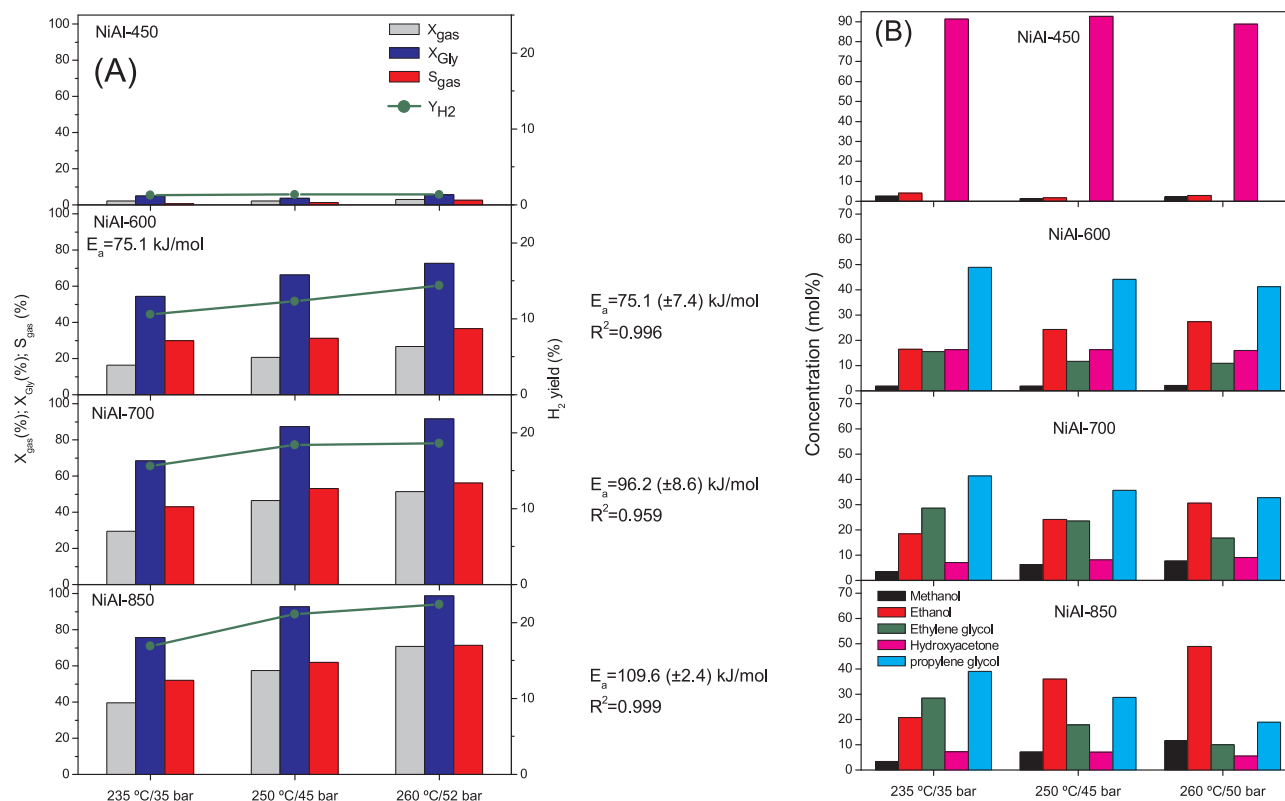
Fig. 9. Effect of operation conditions (T/P) on the catalyst performance: (A) gas phase, and (B) liquid phase.

and selectivity to gas) as a function of time-on-stream (TOS) was investigated for catalysts NiAl-700 and NiAl-850, under mild conditions (235 °C/35 bar) for a period of 50 h. As shown in Fig. 10 both catalysts followed a similar trend, with a sustained loss of activity over the whole catalytic test, being more pronounced during the first hours of operation (i.e. 8 h TOS). An overall decay of around 45% and 60% was observed in the glycerol conversion and conversion to gas, respectively. S_{gas} also decreased with TOS, and after 20 h, it levelled-off at around 61% and 73% for NiAl-700 and NiAl-850, respectively. The stability of these catalysts can be deemed as good as compared to other nickel supported catalysts. For example, Shabaker et al. [45] reported 90% of initial activity decay during 48 h of APR of ethylene glycol over Ni supported on different supports, among them γ-alumina, and attributed to metal sintering. Thus, catalysts prepared by activation of spinel-based precursors showed promising stability results, as compared to traditional impregnation methods.

Fig. 11 depicts the evolution with TOS of several reaction parameters related to the selectivity of the APR reaction of NiAl-700 and NiAl-850 catalysts. Selectivity to hydrogen increased, particularly after 20–30 h of TOS. The yield to hydrogen, however, remained stable due to the counter effect of the loss of activity. Concomitantly, selectivity to methane decreased as reaction proceed, particularly for NiAl-700 (Figs. 11A and B).

The total molar flow of gaseous products dropped-off by around 26% for both catalysts after 50 h of operation. The gas stream enriched in hydrogen with TOS, and both H_2/CO_2 and H_2/CH_4 ratios increased (Figs. 11A and B). The opposite trend was observed on H_2/CO, especially for catalyst NiAl-700. H_2/CO decreased by around 36% for catalyst NiAl-850 and up to 65% for NiAl-700. This is consistent with a limited occurrence of WGS as TOS increased. It is known the high CO and CO_2 hydrogenation [71] and WGS [47] activity of metallic Ni. In both reactions, the Ccontaining molecule is firstly activated onto the metallic site [72]. The observed data suggested that the severe hydrothermal conditions of APR inhibit the CO activation capacity of Ni. The

fact that NiAl-700 contained half the amount of Ni° of NiAl-850 would make it more sensitive to deactivation.

Regarding intermediate liquid products, both NiAl-700 and NiAl-850 showed similar trend, where hydroxyacetone formation increased and ethylene glycol, ethanol and methanol decreased with TOS (Fig. 11C). This behaviour revealed a decreasing trend in the (Scheme 1) route A/route B product distribution, which varied from 1.1 to 0.7 for NiAl-700 and from 0.85 to 0.6 for NiAl-850, indicative of a loss of metal function.

3.3. Characterization of spent catalysts

The spent catalysts were analysed in order to elucidate the main factors that contribute to catalyst deactivation. The nickel re-oxidation and lixiviation, the structural changes in the catalysts and the formation of carbonaceous deposits were analysed.

The specific surface area of the spent catalysts increased (Table 1), more markedly for samples reduced at higher temperature. The used samples showed bimodal pore size distribution (Figure S1B, Supporting Information), which would be related to the coexistence of both boehmite and nickel aluminate phases.

H_2-TPR analysis of spent NiAl-T catalysts (named as NiAl-T-u) are shown in Fig. 1B, and the obtained values are given in Table S4, Supporting Information. Catalysts NiAl-300-u showed an incipient peak below 500 °C, indicative of nickel re-oxidation. Samples reduced at T ≥ 600 °C showed a substantial low-temperature hydrogen consumption what reflected that re-oxidation of metallic Ni took place to a greater extent. Reduction at 250 °C suggested coalescence into large NiO particles as due to high free surface energy. The less intense, unresolved peaks in the 300–600 °C range observed for samples NiAl-700 and NiAl-850 were ascribed to the reduction of smaller NiO particles interacting with the support or to nickel defective spinel compounds. The subtle reduction peak of catalyst NiAl-850 at about 750 °C suggested that part of the Ni was re-oxidized to the original spinel
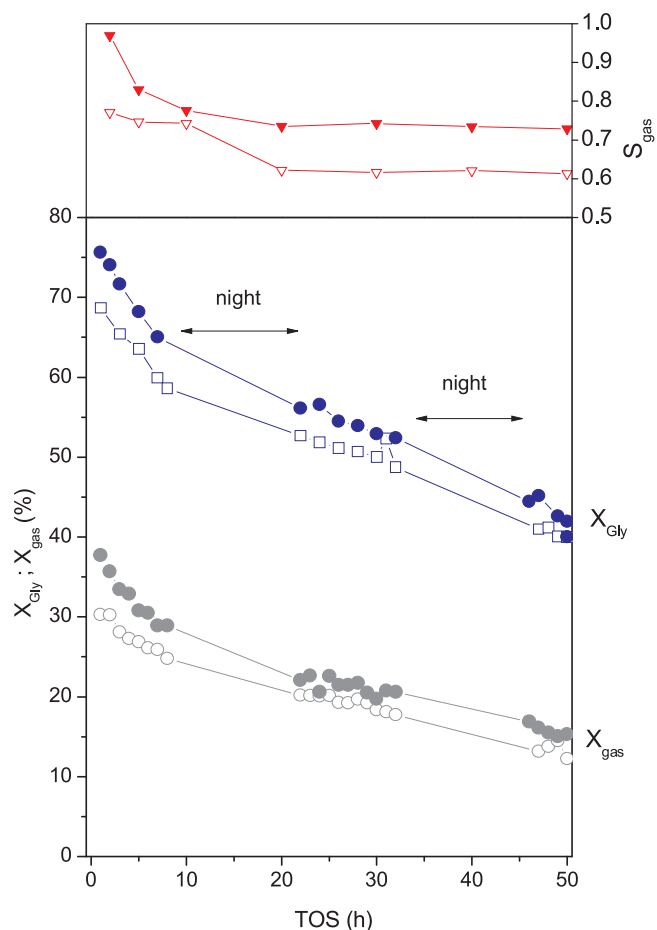
Fig. 10. Evolution of X_{Gly} (blue), X_{gas} (grey) and S_{gas} (red) with TOS. Filled symbols: NiAl-850; Open symbols: NiAl-700. Reaction conditions: 235 °C/ 35 bar (0.5 g of catalysts, feed rate 0.2 mL/min, 10 wt.% glycerol in water mixture, WHSV = 24.5 h^{-1}) (For interpretation of the references to colour in this figure legend, the reader is referred to the web version of this article).

Fig. 11. Variation of reaction indices with TOS. (A) NiAl-700; (B) NiAl-800; (C) Liquid phase indices.

structure, facilitated by the open spinel structure of γ-alumina that hosted the Ni^{2+} species [73]. TPR analyses quantified this amount at around 4.2% of the loaded Ni. Note that the high temperature hydrogen consumption (at around 775 °C) of NiAl-700 indicated the existence of nickel aluminate spinel, yet unreduced in the fresh catalyst. For these most active catalysts, overall, around 45% of the metallic Ni in fresh catalyst was re-oxidised (Table 2). Yet, we have no clear evidence to explain the larger than 100% re-oxidation measured for catalyst NiAl-600. We hypothesize it could be caused by leaching of Ni atoms located in the spinel structure, and subsequent re-deposition on the surface [37,74] employed Ni/alumina prepared by wetness impregnation for the ethylene glycol reforming, and also acknowledged the nickel oxidation as the main cause of deactivation.

The reduction profiles of catalysts used for 50 h (NiAl-700-50 h and NiAl-850-50 h, Fig. 1B) were qualitatively very similar to those used for 2 h. In the spent catalyst, around 34% of the initial Ni was re-oxidized, what indicated that most of the metallic Ni in our catalytic system was oxidized during initial stages of APR. This would explain the previously noted initial fast activity decay (Fig. 10). Thereafter, these species were progressively leached out, and around 7% of the metal loaded was lost during the long-term catalytic run (Table 1).

XRD analysis of the used samples revealed the presence of boehmite phase (Fig. 2B, Table 1) in spent catalysts. The characteristic peaks intensity increased with reduction temperature, probably due to increasing content of γ-Al$_2$O$_3$ in fresh catalysts and its transformation into boehmite. Indeed, the acidity of the reaction medium increased with

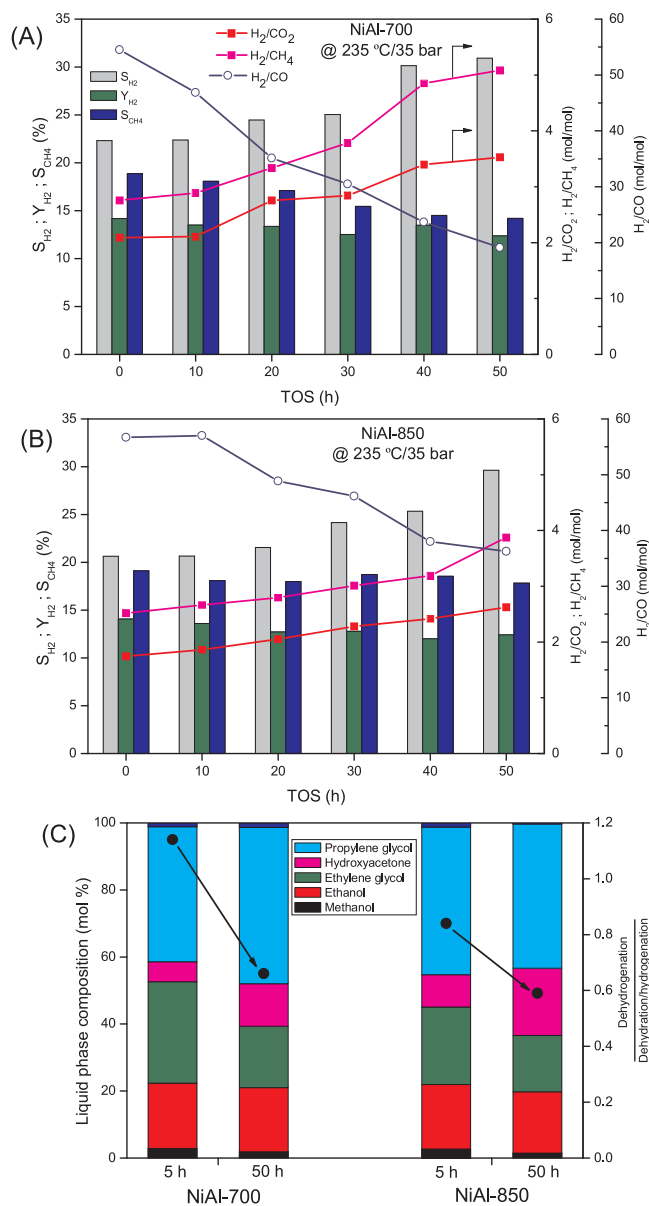time (feed pH: 8; collected liquid product after 2 h TOS pH: 4, as due to the dissolved CO$_2$), enhancing the hydration of γ-alumina. Formation of boehmite was also confirmed by FTIR of the spent catalysts (Figure S3B, Supporting Information). For the samples reduced at 700 and 850 °C, NiO was also detected by XRD, which confirmed the re-oxidation of nickel surface, in agreement with TPR results.

The amount of exposed Ni area dramatically dropped after APR tests (Table 2). For example, the exposed Ni area for the most active catalyst NiAl-850 decreased from 3.47 m^2/g (fresh catalyst) to 0.23 m^2/g (2 TOS), what represents a 93% decrease. However, the observed leaching and particle migration and sinterization cannot explain such a drop in the exposed area. This observation could be the result of the formation of core-shell particles under APR conditions [75], comprised of metallic Ni core and metal oxide shell. The catalytic activity decay was in line with the amount of re-oxidized Ni as measured from TPR analysis.

Regarding the nickel particle growth, it occurred rapidly, as determined by XRD analysis. For example, after two hours of TOS, particle size increased from around 8–14 nm to 42–46 nm (Table 1). Thereafter, it did not substantially increase after 50 h of usage (for example, for

NiAl-850 catalyst, metallic nickel crystallite size was 44.1 nm). The opposite trend observed for NiAl-700 catalyst suggests leaching of larger particles, what is in direct contradiction with that reported by others where small particles are main source of leached species [74]. Nickel particles of NiAl-600 with the initial smaller particle size outgrow those of samples NiAl-700 and NiAl-850, and all the spent catalysts ended up with similar particle size. This is consistent with theories on particle migration [74] where the initial particle growth rate is larger for smaller particles, and the rates decrease as the average particle size increases. It appeared that the average Ni particle size of spent catalysts was not significantly affected by the activation temperature. However, a subtle decreasing trend could be deduced as reduction temperature increased, what could be ascribed to stronger interaction of Ni particles with the support.

Leaching of Ni and Al was also considered given the acidity of the reaction medium (pH decreased to 4 with TOS). The ICP data (Table 1) revealed that leaching of Al from the support was negligible. Leaching of Ni occurred during APR, however, it was minimal even under high glycerol conversion conditions (i.e. about 0.2% Ni leached for NiAl-850 catalyst).

Spent catalyst after 50 h TOS contained small amounts of carbonaceous deposits (0.2–1.0 mmol$_C$/g) (Table 1), lesser than typical values reported in the literature (up to 10 mmol$_C$/g) [61,76], which makes the nickel aluminate spinel-derived catalysts resistant to deactivation by coke. Morever, XRD of spent catalysts (Fig. 2B) showed the absence of diffraction peaks of graphitic carbon, reflecting its low content.

Based on the characterisation of spent catalysts, it seemed that the main causes of activity decay were nickel re-oxidation and sintering, while metal leaching and coke formation had subtle effect.

4. Conclusions

Stoichiometric bulk nickel aluminate spinel was prepared by coprecipitation and calcination at 850 °C. The effect of reduction temperature, between 300 and 850 °C, on physichochemical properties and catalytic performance in the APR of glycerol were investigated.

Results clarify that pore volume was hardly affected upon reduction (300–850 °C), with minor alterations in specific area and average pore size. Also, XRD, DRS-UV and FTIR analyses confirmed the good stability of the spinel structure. The used coprecipitation method led to defective Ni-Al mixed oxides, where metallic nickel diffused to the solid surface, strongly interacting with the bulk, what provided very small metallic nickel particles (< 14 nm). It was noticed that hydrogen treatment increased surface density of medium strength acid and basic sites, in detriment of weak and strong sites.

It is remarkable the high performance shown by our nickel aluminate catalysts in glycerol APR, in spite of the high space velocity (WHSV 24.5 h^{-1}). The most active assay was that reduced at 850 °C with 93% glycerol conversion, 57% conversion to gas and 62% selectivity to gas (at 250 °C/45 bar). The maximum specific hydrogen production rate was achieved upon reduction at 600 °C, due to adequate ratio between Ni° and accessible support.

For all the prepared assays, hydrogen was the main compound in the gaseous stream, followed by carbon dioxide and methane. The low formation of CO suggested that WGS was also favoured by our NiAl$_2$O$_4$-derived catalysts to form H$_2$ and CO$_2$. Other small chain alkanes were hardly detected what evidenced the high C-C scission ability of the investigated catalysts.

Reduction temperature had a more marked effect on the liquid phase product distribution. Results suggested a key contribution of accessible metallic sites and medium strength acidic sites to the overall reaction scheme, with the glycerol reforming occurring through both the dehydrogenation to glyceraldehyde, and through dehydration of terminal hydroxyl groups, and subsequent hydrogenation to yield 1,2-propylene glycol. Activation at 700 °C or above favoured dehydrogenation mechanism, whereas dehydration/hydrogenation mechanism was dominant for catalysts reduced below 600 °C.

Long term catalytic runs revealed the good durability of Ni aluminate spinel catalysts, where deactivation occurred mainly though nickel re-oxidation and sinterization, which, indeed, modified the distribution of gas and intermediate liquid products with TOS.

Acknowledgements

Appendix A. Supplementary data

Supplementary material related to this article can be found, in the online version, at doi:https://doi.org/10.1016/j.apcatb.2018.12.020.

References

[1] L.C. Meher, D. Vidya Sagar, S.N. Naik, Technical aspects of biodiesel production by transesterification-a review, Renew. Sust. Energ. Rev. 10 (3) (2006) 248–268.

[2] G.T. Jeong, H.S. Yang, D.H. Park, Optimization of transesterification of animal fat ester using response surface methodology, Bioresour. Technol. 100 (1) (2009) 25–30.

[3] M.I. Al-Widyan, A.O. Al-Shyoukh, Experimental evaluation of the transesterification of waste palm oil into biodiesel, Bioresour. Technol. 85 (3) (2002) 253–256.

[4] R. Ciriminna, C. Della Pina, M. Rossi, M. Pagliaro, Understanding the glycerol market, Eur. J. Lipid Sci. Technol. 116 (2014) 1432–1439.

[5] C.H. Zhou, J.N. Beltramini, Y.X. Fan, G.Q. Lu, Chemoselective catalytic conversion of glycerol as a biorenewable source to valuable commodity chemicals, Chem. Soc. Rev. 37 (2008) 527–549.

[6] N.H. Tran, G.S. Kannangara, Conversion of glycerol to hydrogen rich gas, Chem. Soc. Rev. 42 (24) (2013) 9454–9479.

[7] R.D. Cortright, R.R. Davda, J.A. Dumesic, Hydrogen from catalytic reforming of biomass-derived hydrocarbons in liquid water, Nature 418 (2002) 964–967.

[8] R.R. Davda, J.W. Shabaker, G.W. Huber, R.D. Cortright, J.A. Dumesic, A review of catalytic issues and process conditions for renewable hydrogen and alkanes by aqueous-phase reforming of oxygenated hydrocarbons over supported metal catalysts, Appl. Catal. B:Environ. 56 (2005) 171–186.

[9] M. El Doukkali, A. Iriondo, P.L. Arias, J. Requies, I. Gandarías, L. Jalowiecki-Duhamel, F. Dumeignil, A comparison of sol–gel and impregnated Pt or/and Ni based γ-alumina catalysts for bioglycerol aqueous phase reforming, Appl. Catal. B:Environ. 125 (2012) 516–529.

[10] Y.C. Lin, Review: catalytic valorization of glycerol to hydrogen and syngas, Int. J. Hydrogen Energ. 38 (6) (2013) 2678–2700.

[11] R.L. Manfro, A.F. da Costa, N.F.P. Ribeiro, M.M.V.M. Souza, Hydrogen production by aqueous-phase reforming of glycerol over nickel catalysts supported on CeO$_2$, Fuel process, Technol. 92 (3) (2011) 330–335.

[12] G. Wen, Y. Xu, H. Ma, Z. Xu, Z. Tian, Production of hydrogen by aqueous-phase reforming of glycerol, Int. J. Hydrogen Energ. 33 (22) (2008) 6657–6666.

[13] R.L. Manfro, T.P.M.D. Pires, N.F.P. Ribeiro, M.M.V.M. Souza, Aqueous-phase reforming of glycerol using Ni–Cu catalysts prepared from hydrotalcite-like precursors, Catal. Sci. Technol. 3 (2013) 1278–1287.

[14] A. Iriondo, V.L. Barrio, J.F. Cambra, P.L. Arias, M.B. Güemez, R.M. Navarro, M.C. Sánchez-Sánchez, J.L.G. Fierro, Hydrogen production from glycerol over nickel catalysts supported on Al$_2$O$_3$ modified by Mg, Zr, Ce or La, Top. Catal. 49 (1) (2008) 46–58.

[15] J. Remón, J.R. Giménez, A. Valiente, L. García, J. Arauzo, Production of gaseous and liquid chemicals by aqueous phase reforming of crude glycerol: influence of operating conditions on the process, Energy Convers. Manag. 110 (2016) 90–112.

[16] A. Seretis, P. Tsiakaras, Crude bio-glycerol aqueous phase reforming and hydrogenolysis over commercial SiO$_2$-Al$_2$O$_3$ nickel catalyst, Renew. Energ. 97 (2016) 373–379.

[17] Y. Kathiraser, W. Thitsartarn, K. Sutthiumporn, S. Kawi, Inverse NiAl$_2$O$_4$ on LaAlO$_3$–Al$_2$O$_3$: unique catalytic structure for stable CO$_2$ reforming of methane, J. Phys. Chem. C 117 (16) (2013) 8120–8130.

[18] R.M. Ravenelle, J.R. Copeland, W.G. Kim, John C. Crittenden, C. Sievers, Structural changes of γ-Al$_2$O$_3$-Supported catalysts in hot liquid water, ACS Catal. 1 (5) (2011) 552–561.

[19] C. Jiménez-González, Z. Boukha, B. de Rivas, J.J. Delgado, M.A. Cauqui, J.R. González-Velasco, J.I. Gutiérrez-Ortiz, R. López-Fonseca, Structural characterisation of Ni/alumina reforming catalysts activated at high temperatures, Appl. Catal. A:Gen. 466 (2013) 9–20.

[20] H. Özdemir, M.A.F. Öksüzömer, M.A. Gürkaynak, Effect of the calcination temperature on Ni/MgAl$_2$O$_4$ catalyst structure and catalytic properties for partial oxidation of methane, Fuel 116 (2014) 63–70.

[21] H.S.C. O'Neill, W.A. Dollase, C.R. Ross II, Temperature dependence of the cation

distribution in nickel aluminate (NiAl$_2$O$_4$) spinel: a powder XRD study, Phys. Chem. Minerals 18 (1991) 302–319.

[22] A. Khan, P.G. Smirniotis, Relationship between temperature-programmed reduction profile and activity of modified ferrite-based catalysts for WGS reaction, J. Mol. Catal. A:Chem. 280 (1–2) (2008) 43–51.

[23] F.P. Ribeiro, R.C.R. Neto, S.F. Moya, M.M.V.M. Souza, M. Schmal, Synthesis of NiAl$_2$O$_4$ with high surface area as precursor of Ni nanoparticles for hydrogen production, Int. J. Hydrogen Energ. 35 (21) (2010) 11725–11732.

[24] Z. Boukha, C. Jiménez-González, B. de Rivas, J.R. González-Velasco, J.I. Gutiérrez-Ortiz, R. López-Fonseca, Synthesis, characterisation and performance evaluation of spinel-derived Ni/Al$_2$O$_3$ catalysts for various methane reforming reactions, Appl. Catal. B:Environ. 158–159 (2014) 190–201.

[25] M.C.J. Bradford, M.A. Vannice, Catalytic reforming of methane with carbon dioxide over nickel catalysts II. Reaction kinetics, Appl. Catal. A:Gen. 142 (1996) 97–122.

[26] J.S. Smith, P.A. Thrower, M.A. Vannice, Characterization of NiTiO$_2$ catalysts by TEM, X-ray diffraction, and chemisorption techniques, J. Catal. 68 (1981) 270–285.

[27] J.C. Ganley, F.S. Thomas, E.G. Seebauer, R.I. Masel, A priori catalytic activity correlations: the difficult case of hydrogen production from Ammonia, Catal. Lett. 96 (2004) 117.

[28] C.H. Bartholomew, Mechanisms of catalyst deactivation, Appl. Catal. A:Gen. 212 (1–2) (2001) 17–60.

[29] G. Li, L. Hu, J.M. Hill, Comparison of reducibility and stability of alumina-supported Ni catalysts prepared by impregnation and co-precipitation, Appl. Catal. A:Gen. 301 (1) (2006) 16–24.

[30] J.L. Rogers, M.C. Mangarella, A.D. D'Amico, J.R. Gallagher, M.R. Dutzer, E. Stavitski, J.T. Miller, C. Sievers, Differences in the nature of active sites for methane dry reforming and methane steam reforming over nickel aluminate catalysts, ACS Catal. 6 (9) (2016) 5873–5886.

[31] A. Tirsoaga, D. Visinescu, B. Jurca, A. Ianculescu, O. Carp, Eco-friendly combustion-based synthesis of metal aluminates MAl$_2$O$_4$ (M 5 Ni, Co), J. Nanopart. Res. 13 (2011) 6397–6408.

[32] L. Zhou, L. Li, N. Wei, J. Li, J.M. Basset, Effect of NiAl$_2$O$_4$ formation on Ni/Al$_2$O$_3$ stability during dry reforming of methane, ChemCatChem 7 (16) (2015) 2508–2516.

[33] Z. Skoufa, G. Xantri, E. Heracleous, A.A. Lemonidou, A study of Ni–Al–O mixed oxides as catalysts for the oxidative conversion of ethane to ethylene, Appl. Catal. A:Gen. 471 (2014) 107–117.

[34] N. Braidy, S. Bastien, J. Blanchard, C. Fauteux-Lefebvre, I.E. Achouri, N. Abatzoglou, Activation mechanism and microstructural evolution of a YSZ/Ni-alumina catalyst for dry reforming of methane, Catal. Today 291 (2017) 99–105.

[35] J. Zhang, H. Xu, X. Jin, Q. Ge, W. Li, Characterizations and activities of the nano-sized Ni/Al$_2$O$_3$ and Ni/La–Al$_2$O$_3$ catalysts for NH$_3$ decomposition, Appl. Catal. A Gen. 290 (1–2) (2005) 87–96.

[36] Y.S. Han, J.B. Li, X.S. Ning, B. Chi, Effect of preparation temperature on the lattice parameter of nickel aluminate spinel, J. Am. Ceram. Soc. 87 (7) (2004) 1347–1349.

[37] G. Wen, Xu Y, Z. Xu, Z. Tian, Characterization and catalytic properties of the Ni/Al$_2$O$_3$ catalysts for aqueous-phase reforming of glucose, Catal. Lett. 129 (2009) 250–257.

[38] E. Heracleous, A.F. Lee, K. Wilson, A.A. Lemonidou, Investigation of Ni-based alumina-supported catalysts for the oxidative dehydrogenation of ethane to ethylene: structural characterization and reactivity studies, J. Catal. 231 (1) (2005) 159–171.

[39] J. Wang, L. Dong, Y. Hu, G. Zheng, Z. Hu, Y. Chen, Dispersion of NiO supported on γ-Al$_2$O$_3$ and TiO$_2$/γ-Al$_2$O$_3$ supports, J. Solid State Chem. 157 (2) (2001) 274–282.

[40] J.L. Cuya Huaman, N. Hironaka, S. Tanaka, K. Shinoda, H. Miyamura, B. Jeyadevan, Size-controlled monodispersed nickel nanocrystals using 2-octanol as reducing agent, CrystEngComm 15 (2013) 729–737.

[41] A. Tribalis, G.D. Panagiotou, K. Bourikas, L. Sygellou, S. Kennou, S. Ladas, A. Lycourghiotis, C. Kordulis, Ni catalysts supported on modified alumina for diesel steam reforming, Catalysts 6 (1) (2016) 11–24.

[42] H. Deng, Y. Yu, H. He, The role of AgOAl entities in adsorption of NCO species and reduction of NOx, Catal Today 258 (1) (2015) 35–40.

[43] R. Estevez, S. Lopez-Pedrajas, F. Blanco-Bonilla, D. Luna, F.M. Bautista, Production of acrolein from glycerol in liquid phase on heterogeneous catalysts, Chem. Eng. J. 282 (2015) 179–186.

[44] B.C. Miranda, R.J. Chimentão, F. Gispert-Guirado, J. Llorca, F. Medina, F. LópezBonillo, J.E. Sueiras, Conversion of glycerol over 10%Ni/γ-Al$_2$O$_3$ catalyst, Appl. Catal. B:Environ. 147 (2014) 464–480.

[45] J.W. Shabaker, G.W. Huber, J.A. Dumesic, Aqueous-phase reforming of oxygenated hydrocarbons over Sn-modified Ni catalysts, J. Catal. 222 (1) (2004) 180–191.

[46] E.B. Pereira, N. Homs, S. Martí, J.L.G. Fierro, P. Ramírez de la Piscina, Oxidative steam-reforming of ethanol over Co/SiO$_2$, Co-Rh/SiO$_2$ and Co-Ru/SiO$_2$ catalysts: catalytic behavior and deactivation/regeneration processes, J. Catal. 257 (1) (2008) 206–214.

[47] D.C. Grenoble, M.M. Estadt, D.F. Ollis, The chemistry and catalysis of the water gas shift reaction: 1. The kinetics over supported metal catalysts, J. Catal. 67 (1) (1981) 90–102.

[48] J.R. Rostrup-Nielsen, Catalytic Steam Reforming, Springer-Verlag, Berlin, 1984.

[49] F. Bastan, M. Kazemeini, A. Larimi, H. Maleki, Production of renewable hydrogen through aqueous-phase reforming of glycerol over Ni/Al2O3MgO nano-catalyst, Int. J. Hydrogen Energ. 43 (2) (2018) 614–662.

[50] Y.H. Park, J.Y. Kim, D.J. Moon, N.C. Park, Y.C. Kim, Effect of LaAlO$_3$-supported modified Ni-based catalysts on aqueous phase reforming of glycerol, Res. Chem. Intermediat. 41 (12) (2015) 9603–9614.

[51] M.M. Rahman, T.L. Church, M.F. Variava, A.T. Harris, A.I. Minett, Bimetallic Pt–Ni composites on ceria-doped alumina supports as catalysts in the aqueous-phase reforming of glycerol, RSC Adv. 4 (2014) 18951–18960.

[52] F. Bastan, M. Kazemeini, A.S. Larimi, Aqueous-phase reforming of glycerol for production of alkanes over Ni/Ce$_x$Zr$_{1-x}$O$_2$ nano-catalyst: effects of the support's composition, Renew. Energ. 108 (2017) 417–424.

[53] D.L. King, L. Zhang, G. Xia, A.M. Karim, D.J. Heldebrant, X. Wang, T. Peterson, Y. Wang, Aqueous phase reforming of glycerol for hydrogen production over Pt–Re supported on carbon, Appl. Catal B: Environ. 99 (1-2) (2010) 206–213.

[54] C. Pendem, B. Sarkar, N. Siddiqui, L.N.S. Konathala, C. Baskar, R. Bal, K-promoted Pt-hydrotalcite catalyst for production of H2 by aqueous phase reforming of glycerol, ACS Sustainable Chem. Eng. 6 (2) (2018) 2122–2131.

[55] Y. Guo, M.U. Azmat, X. Liu, Y. Wang, G. Lu, Effect of support's basic properties on hydrogen production in aqueous-phase reforming of glycerol and correlation between WGS and APR, Acs Appl. Energy Mater. 92 (2012) 218–223.

[56] S. Liu, M. Tamura, Z. Shen, Y. Zhang, Y. Nakagawa, K. Tomishige, Hydrogenolysis of glycerol with in-situ produced H2 by aqueous-phase reforming of glycerol using Pt-modified Ir-ReOx/SiO$_2$ catalyst, Catal. Today 303 (2018) 106–116.

[57] G.W. Huber, R.D. Cortright, J.A. Dumesic, Renewable alkanes by aqueous-phase reforming of biomass-derived oxygenates, Angew. Chem. Int. Ed. 43 (12) (2004) 1549–1551.

[58] A. Ciftci, S. Eren, D.A.J.M. Ligthart, E.J.M. Hensen, Platinum-rhenium synergy on reducible oxide supports in aqueous phase glycerol reforming, ChemCatChem 6 (2014) 1260–1269.

[59] L. Bobrova, D. Andreev, E. Ivanov, N. Mezentseva, L. Simonov, A. Gribovskii, V. Sadykov, Water-gas shift reaction over Ni/CeO$_2$ Catalysts, Catalysts 7 (10) (2017) 310–334.

[60] L.I. Godina, A.V. Tokarev, I.L. Simakova, P. Mäki-Arvela, E. Kortesmäki, J. Gläsel, L. Kronberg, B. Etzold, D.Y. Murzin, Aqueous-phase reforming of alcohols with three carbon atoms on carbon-supported Pt, Catal. Today 301 (2018) 78–89.

[61] N.Luo.X. Fu, F. Cao, T. Xiao, P.P. Edwards, Glycerol aqueous phase reforming for hydrogen generation over Pt catalyst – effect of catalyst composition and reaction conditions, Fuel 87 (17–18) (2008) 3483–3489.

[62] A. Talebian-Kiakalaieh, N.A.S. Amin, H. Hezaveh, Glycerol for renewable acrolein production by catalytic dehydration, Renew. Sust. Energ. Rev. 40 (2014) 28–59.

[63] I. Gandarias, P.L. Arias, J. Requies, M.B. Güemez, J.L.G. Fierro, Hydrogenolysis of glycerol to propanediols over a Pt/ASA catalyst: the role of acid and metal sites on product selectivity and the reaction mechanism, Appl. Catal. B:Environ. 97 (1-2) (2010) 248–256.

[64] Y.S. Yun, D.S. Park, J. Yi, Effect of nickel on catalytic behaviour of bimetallic Cu-Ni catalyst supported on mesoporous alumina for the hydrogenolysis of glycerol to 1,2-propanediol, Catal. Sci. Technol. 4 (2014) 3191–3202.

[65] I. Gandarias, J. Requies, P.L. Arias, U. Armbruster, A. Martin, Liquid-phase glycerol hydrogenolysis by formic acid over Ni-Cu/Al$_2$O$_3$ catalysts, J. Catal. 290 (2012) 79–89.

[66] I. Gandarias, P.L. Arias, J. Requies, M. El Doukkali, M.B. Güemez, Liquid-phase glycerol hydrogenolysis to 1,2-propanediol under nitrogen pressure using 2-propanol as hydrogen source, J. Catal. 282 (1) (2011) 237–247.

[67] A.K. Agarwal, M.S. Wainwright, D.L. Trimm, N.W. Cant, Acetaldehyde hydrogenation over a Cu/SiO2 catalyst, J. Mol. Catal. 45 (2) (1988) 247–254.

[68] A.V. Kirilin, A.V. Tokarev, E.V. Murzin, L.M. Kustov, J.P. Mikkola, D.Y. Murzin, Reaction products and transformations of intermediates in the aqueous phase reforming of sorbitol, ChemSusChem 3 (6) (2010) 708–718.

[69] A. Seretis, P. Tsiakaras, Aqueous phase reforming (APR) of glycerol over platinum supported on Al$_2$O$_3$ catalyst, Renew. Energy 85 (2016) 1116–1126.

[70] M.A. Dasari, P.P. Kiatsimkul, W.R. Sutterlin, G.J. Suppes, Low-pressure hydrogenolysis of glycerol to propylene glycol, Appl. Catal. A:Gen. 281 (1–2) (2005) 225–231.

[71] V. Shadravan, E. Kennedy, M. Stockenhuber, An experimental investigation on the effects of adding a transition metal to Ni/Al$_2$O$_3$ for catalytic hydrogenation of CO and CO$_2$ in presence of light alkanes and alkenes, Catal. Today 307 (2018) 277–285.

[72] J. Sehested, S. Dahl, J. Jacobsen, J.R. Rostrup-Nielsen, Methanation of CO over nickel: mechanism and kinetics at high H$_2$/CO ratios, J. Phys. Chem. B 109 (6) (2005) 2432–2438.

[73] F. Aupretre, C. Descorme, D. Duprez, D. Casanave, D. Uzio, Ethanol steam reforming over Mg$_X$Ni$_{1-X}$Al$_2$O$_3$ spinel oxide-supported Rh catalysts, J. Catal. 233 (2) (2005) 464–477.

[74] T. van Haasterecht, M. Swart, K.P. de Jong, J.H. Bitter, Effect of initial nickel particle size on stability of nickel catalysts for aqueous phase reforming, J. Energy Chem. 25 (2) (2016) 289–296.

[75] M. El Doukkali, A. Iriondo, J.F. Cambra, I. Gandarias, L. Jalowiecki-Duhamel, F. Dumeignil, P.L. Arias, Deactivation study of the Pt and/or Ni-based γ-Al$_2$O$_3$ catalysts used in the aqueous phase reforming of glycerol for H$_2$ production, Appl. Catal. A:Gen. 472 (2014) 80–91.

[76] A. Iriondo, J.F. Cambra, V.L. Barrio, M.B. Guemez, P.L. Arias, M.C. Sanchez-Sanchez, R.M. Navarro, J.L.G. Fierro, Glycerol liquid phase conversion over monometallic and bimetallic catalysts: Effect of metal, support type and reaction temperatures, Appl. Catal. B:Environ. 106 (1–2) (2011) 83–93.